

2008

## Characterization of temperature dependent nonlinear optical properties of semiconductor materials

Vincent M. Cowan  
*University of Dayton*

Follow this and additional works at: [https://ecommons.udayton.edu/graduate\\_theses](https://ecommons.udayton.edu/graduate_theses)

---

### Recommended Citation

Cowan, Vincent M., "Characterization of temperature dependent nonlinear optical properties of semiconductor materials" (2008). *Graduate Theses and Dissertations*. 2134.  
[https://ecommons.udayton.edu/graduate\\_theses/2134](https://ecommons.udayton.edu/graduate_theses/2134)

This Thesis is brought to you for free and open access by the Theses and Dissertations at eCommons. It has been accepted for inclusion in Graduate Theses and Dissertations by an authorized administrator of eCommons. For more information, please contact [mschlangen1@udayton.edu](mailto:mschlangen1@udayton.edu), [ecommons@udayton.edu](mailto:ecommons@udayton.edu).

**CHARACTERIZATION OF TEMPERATURE DEPENDENT NONLINEAR  
OPTICAL PROPERTIES OF SEMICONDUCTOR MATERIALS**

Thesis

Submitted to

The School of Engineering of the  
UNIVERSITY OF DAYTON

in Partial Fulfillment of the Requirements for

The Degree

Master of Engineering in Electro-Optics

by

Vincent M. Cowan

UNIVERSITY OF DAYTON

Dayton, Ohio

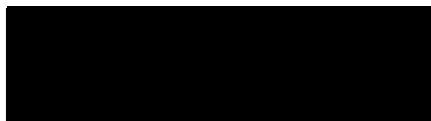
March, 2008

CHARACTERIZATION OF TEMPERATURE DEPENDENT NONLINEAR  
OPTICAL PROPERTIES OF SEMICONDUCTOR MATERIALS

APPROVED BY:



Peter E. Powers, Ph.D.  
Professor,  
Electro-Optics Program  
University of Dayton  
Committee Chairman



Joseph W. Haus, Ph.D.  
Professor  
Electro-Optics Program  
University of Dayton  
Committee Member



Leonel P. Gonzalez, M.S.  
Principal Scientist  
Materials Directorate  
Air Force Research Lab  
Committee Member



Shekhar Guha, Ph.D.  
Principal Scientist  
Materials Directorate  
Air Force Research Lab  
Committee Member



Joel M. Murray, Ph.D.  
Principal Scientist  
Materials Directorate  
Air Force Research Lab  
Committee Member



Joseph E. Saliba, Ph.D, PE  
Dean  
School of Engineering



Malcolm W. Daniels, Ph.D.  
Associate Dean  
School of Engineering

## Abstract

### **CHARACTERIZATION OF TEMPERATURE DEPENDENT NONLINEAR OPTICAL PROPERTIES OF SEMICONDUCTOR MATERIALS**

Vincent M. Cowan  
University of Dayton

Advisor: Dr. Peter E. Powers

If a material is to be used for an optical application, it is important to know its refractive index and absorption coefficient for both the linear and nonlinear cases. Most nonlinear optical properties of semiconductors are characterized near room temperature because of the relative ease of measurement which it affords. Examining the temperature dependence of semiconductor optical nonlinearities introduces complications when using standard measurement techniques, especially at low temperatures since a cryostat must be used. The use of a bulky cryostat with its associated vacuum/electrical lines can prove to be difficult when using measurement techniques that require translation of the sample. Furthermore, sample translation can prove challenging when characterizing novel materials which are often wedged. When wedged material are translated beam walking can result. An Irradiance scan technique was utilized in this research keeping the sample fixed within a cryostat allowing the nonlinear optical properties to be measured at both room and cryogenic temperatures with relative ease.

Measurements were conducted at a fixed wavelength of 1.064  $\mu\text{m}$  and the measurements focused on determining the free carrier refraction coefficient, nonlinear refractive index, and the two photon absorption coefficient of semiconductors. The nonlinearities were determined by simultaneously measuring the on-axis fluence and total transmitted energy through a sample at varying incident irradiances. A finite difference method and curve fitting routine were applied to determine the values of the nonlinear optical properties of GaAs, CdTe, and InP at both 300 and 77 K. The optical nonlinearities for these semiconductors were previously measured at 300 K, and to the best of our knowledge this is first time they were measured 77 K.

## **Acknowledgments**

I would like to thank Dr. Joel Murray, Mr. Leonel Gonzalez, Dr. Shekhar Guha, and the rest of the people in the IR Lab at the Air Force Research Laboratory for their overall guidance, encouragement, advice, and answers while completing this research. I would also like to thank my advisor Dr. Peter Powers at the University of Dayton for his assistance.

## Table of Contents

Abstract.....	iii
Acknowledgements .....	v
Table of Contents.....	vi
List of Illustrations .....	viii
List of Tables.....	ix
Chapter 1 Introduction.....	1
1.1 Background .....	1
1.2 Research Importance .....	3
1.3 Research Focus .....	3
1.4 Research Challenges .....	4
1.5 Research Objective .....	5
1.6 Methodology .....	6
Chapter 2 Background and Nonlinear Optical Property Measurement Techniques .....	7
2.1 Nonlinear Absorption and Refraction, A Brief Review .....	7
2.2 Different Measurement Methods .....	9
2.3 Research Goals and Experimental Considerations .....	14
2.4 Experimental Method.....	17
Chapter 3 Irradiance Scan Theory .....	21
3.1 Nonlinear Beam Propagation in a Semiconductor .....	21
3.2 Analysis and Assumptions.....	22
3.3 Determining $\beta$ .....	23
3.4 Determining $\gamma$ and $\sigma_r$ .....	23
Chapter 4 Overview of Materials Characterized.....	26
4.1 Materials Selected for Characterization .....	26
4.2 Material Applications Overview.....	27
4.3 Material Characterization Values from Literature.....	29
4.4 Uncharacterized Optical Properties .....	31
Chapter 5 Results .....	34
5.1 Definition of Error in Measurements .....	34
5.2 Verification of Test Bed's Accuracy .....	35
5.3 Measured NLA & NLR of GaAs .....	37
5.4 Measured NLA & NLR of InP.....	40
5.5 Measured NLA & NLR of CdTe .....	43
5.6 Final Results Discussion.....	45
Chapter 6 System Performance & Accuracy .....	48

6.1 Introduction.....	48
6.2 Linearity of Detection System .....	48
6.3 Reproducibility .....	50
6.4 Accuracy of Model .....	52
Chapter 7 Conclusions.....	56
7.1 Accomplishments .....	56
7.2 Future Goals.....	57
References.....	60



## List of Illustrations

Figure 2.1: Two photon absorption process .....	9
Figure 2.2: Diagram of negative lensing effect.....	11
Figure 2.3: Cryostat, dewar, and required electrical/vacuum lines .....	15
Figure 2.4: Beam walking illustration.....	16
Figure 2.5: Z-Scan optical schematic.....	17
Figure 2.6: I-scan optical schematic.....	18
Figure 2.7: Optical test bed designed and implemented .....	19
Figure 3.1: Nonlinear beam propagation schematic.....	24
Figure 5.1: CS <sub>2</sub> NLA, and NLR at 300 K .....	36
Figure 5.2: GaAs spectra at 300 K and 77K.....	37
Figure 5.3: GaAs NLA, and NLR at 300 K.....	38
Figure 5.4: GaAs NLA, and NLR at 77 K.....	39
Figure 5.5: InP spectra at 300 K and 77 K .....	41
Figure 5.6: InP NLA, and NLR at 300 K .....	41
Figure 5.7: InP NLA, and NLR at 77 K .....	42
Figure 5.8: CdTe spectra at 300 K and 77 K.....	43
Figure 5.9: CdTe NLA, and NLR at 300 K.....	44
Figure 5.10: CdTe NLA, and NLR at 77 K.....	44
Figure 6.1: Total transmitted energy detectors response to varying incident energies .....	49
Figure 6.2: On-axis fluence detectors response to varying incident energies .....	50
Figure 6.3: On-axis fluence detectors response to varying incident energies .....	52
Figure 7.1: 680nm-10μm irradiance scan test bed .....	58

## List of Tables

Table 4.1: Previously measured CS <sub>2</sub> NLR & NLA coefficients .....	30
Table 4.2: Previously measured GaAs, InP, and CdTe NLR & NLA coefficients	31
Table 4.3: Theoretical $\beta$ for GaAs, InP, and CdTe at 300 K and 77 K.....	32
Table 5.1: CS <sub>2</sub> measured NLR.....	36
Table 5.2: GaAs measured NLA, and NLR .....	39
Table 5.3: InP measured NLA, and NLR.....	42
Table 5.4: CdTe measured NLA, and NLR .....	45
Table 7.1: Summary of nonlinear optical properties measured in this research..	46
Table 7.2: Mirror configurations.....	59

# Chapter 1

## Introduction

### 1.1 Background

Dramatic advances have been made in optical technologies over the last century. Many of these innovations were made possible through the development and testing of novel optical materials. Current applications that utilize these materials include integrated optics, optical sensors, and an array of telecommunications applications.

For many of these applications, both the refractive index and absorption coefficient of the material affects the way that the device performs. Many experiments have been developed to characterize the optical and electrical properties of materials. If a material is to be used for an optical or electro-optical application it is important to know its refractive index and absorption coefficient. The output power of lasers has increased over the years, allowing scientists to measure irradiance<sup>A</sup> dependent material properties. When a device is used in an application where high incident irradiances are present, scientists and engineers are interested in the material's nonlinear refraction and absorption values.

---

<sup>A</sup> S.I. units of intensity and irradiance are:  $\text{Intensity} = \frac{\text{Power}}{\text{Unit Solid Angle}}$  and  $\text{Irradiance} = \frac{\text{Power}}{\text{Unit Area}}$ .

While "Intensity" is commonly used in place of "Irradiance" even though this is the term intended, in this manuscript I will use the proper term.

The optical materials of interest fall into a couple of categories. The first type is organic materials which, including many chemical mixtures. Organic materials are used in micro-fabrication applications and medical applications. The second category of materials are inorganics. Materials in this group include crystals, which are useful for frequency conversion applications. Semiconductors are another inorganic material. All of the material groups mentioned that possess these nonlinear optical properties are of particular interest for optical power filtering applications, optical logic gates, and medical applications.

Semiconductors are an interesting material to work with because the nonlinear optical properties can be modified by changing the dopant level. The science of doping semiconductors is a refined process due to a commercial research thrust over the last three decades driven by the computer industry. Much effort has already been put forth in determining how to successfully dope different semiconductors, which greatly benefits optical engineers because these materials can be of optical quality and their optical nonlinearities are 'tunable'. Another reason semiconductor materials are of interest is that it is possible to produce them in large form factors, which lends itself well to optical applications in which devices need areas of several square centimeters. Lastly, for the most part semiconductors are low cost materials and their optical and electrical characteristics can be changed by simply modifying their doping levels. The research presented here will focus on characterizing the nonlinear optical properties of semiconductors at various temperatures.

Most nonlinear optical properties of semiconductors are characterized near room temperature because of the relative ease of measurement which it affords. Examining any temperature dependence of semiconductor optical nonlinearities introduces some complications when using standard measurement techniques. Temperature dependent optical nonlinearities are measured less frequently because the required hardware to make the measurement is a cumbersome addition to an optical test bed.

## **1.2 Research Importance**

It is important to measure temperature dependent optical nonlinearities of semiconductors, particularly nonlinearities at cryogenic temperatures. In the past, temperature dependent nonlinearities of semiconductors<sup>1</sup> have been found, and there is reason to believe there are other uncharacterized semiconductor materials that exhibit this behavior. One of the issues associated with measuring temperature dependent optical nonlinearities is that a method of test has not been developed that allows the characterization to be conducted with relative ease.

Knowledge of the temperature dependence of nonlinear optical properties will allow engineers and scientists to better understand light-matter interactions.

## **1.3 Research Focus**

There are many properties that contribute to the nonlinear optical response of a material. This research was conducted at a wavelength of 1.064  $\mu\text{m}$  and the temporal characteristics of the laser allowed thermal effects such as a change in lattice spacing and electron mobility to be neglected. The

work presented here focused on finding both the free carrier refraction coefficient, nonlinear refractive index, and the two photon absorption coefficient. The emphasis of this research was to find the aforementioned quantities for several semiconductors at different temperatures.

## **1.4 Research Challenges**

One challenge of this project was to develop a new test bed that can measure the optical nonlinearities of a semiconductor at different temperatures. Another research challenge was to avoid laser induced damage to the material under test, the material is exposed to high power laser radiation in order to characterize optical nonlinearities. The experiment needs to be versatile enough to handle the varying size constraints of the different materials under test. The materials available are often non-uniform in size and it is not unusual to have samples that are slightly wedged. The experiment must be flexible enough to handle the size variations and the inherent problems that result from the size variations.

The optical parameters needed to be determined with minimal physical information known about the sample. The thickness, the real part of the index of refraction, and its linear absorption coefficient were determined in a separate experiment using other optical characterization methods. With this limited amount of information the nonlinear refraction terms and the two-photon absorption coefficient must be determined.

The optical nonlinearities must also be determined at various temperatures. It is important to recognize that the sample must be mounted in a

cryostat in order to vary the sample temperature. Cryostats tend to be bulky in nature and there are inherent hardware constraints that come with its use, including associated vacuum/electrical lines required for its operation. The test bed must be able to account for these hardware constraints and allow the experimenter to measure temperature dependent optical nonlinearities with relative ease.

Our intention in characterizing semiconductor optical nonlinearities over a temperature range was to gain a better understanding of the light-matter interactions in semiconductors. With this understanding, potentially better materials could be developed for applications such as optical filtering, optical logic gates, and damage protection. This research will also provide the scientific community a better understanding of the strengths and limitations of materials employed in current technologies.

## **1.5 Research Objective**

The objective of this research is to build a test bed to measure the nonlinear refractive ( $\gamma$  and  $\sigma_r$ ) and the two photon absorption ( $\beta$ ) coefficients of semiconductor materials at room and cryogenic temperatures. A 20 picosecond duration Nd:YAG laser at an operating wavelength of 1.064  $\mu\text{m}$  was utilized in the experiment. The output irradiance of the laser at focus is large enough to observe intensity-dependent optical nonlinearities. The results obtained from this research will provide a greater knowledge of temperature dependent optical nonlinearities of semiconductors. Having a greater understanding of the materials nonlinear optical properties will allow for more accurate use of these

materials in future theoretical calculations, experimentation, and modeling. Ultimately the experiment will cover the wavelength spectrum of 532nm-10.0 $\mu$ m over a large temperature range. This will provide an excellent understanding of the nonlinear index of refraction and two photon absorption coefficient dependence on intensity temperature and wavelength.

## **1.6 Methodology**

The nonlinear index of refraction, free carrier refraction, and two photon absorption coefficients were measured indirectly using a technique much like an I-scan. We simultaneously measured the on-axis fluence and total transmitted energy through a sample. The intensity of the beam incident on the sample is varied by rotating a half-wave plate in front of a linear polarizer. The sample is then removed and the process is repeated. The values found here are used to normalize the sample data.

The two photon absorption coefficient is determined directly from the least-squares fit to the data showing the dependence of the total transmitted energy on the incident energy. Now having found the two photon absorption coefficient the nonlinear index of refraction and free carrier refraction coefficient can be found from the on-axis transmitted fluence data using a finite difference method.

The chapter to follow will discuss previous measurement methods used to determine nonlinear optical properties of materials. A brief review of nonlinear optical processes will also be provided.



## Chapter 2

### Background and Nonlinear Optical Property Measurement Techniques

#### ***2.1 Nonlinear Absorption and Refraction, A Brief Review***

When light passes from one medium into another medium refraction occurs; the velocity of the light in the two media differ, and not all of the light is transmitted into the second medium. The complex index of refraction  $\tilde{N}$  is used to describe the interaction of light with the material. Eqn. 2.1,  $\tilde{N}$  has both real and imaginary components.

$$\tilde{N} = n - jk \quad (2.1)$$

In this equation  $n$  is the index of refraction and  $k$  is the extinction coefficient. The index of refraction is defined as

$$n = \frac{c}{v} \quad (2.2)$$

where  $c$  is the speed of light in free space and  $v$  is the phase velocity of light in the medium in which it is propagating.

Linear absorption ( $\alpha$ ) arises from the imaginary part of eqn. 2.1. Absorption is a process whereby a photon is absorbed in the material causing an electron to move from the valance band to the conduction band.

The ability of a material to polarize as a response to an applied electric field is represented in the polarization expansion

$$P = \varepsilon_0 (\chi E + \chi^{(2)} E^2 + \chi^{(3)} E^3 + \dots) \quad (2.3)$$

where  $\varepsilon_0$  is the permittivity of the material. The  $\chi$  term represents linear absorption and refraction. The  $\chi^{(2)}$  varies as a function of the electric field squared and represents second harmonic generation and rectification. The  $\chi^{(3)}$  term represents two photon absorption, nonlinear refraction, and although usually a weak effect third harmonic frequency generation, all of these parameters vary as the electric field cubed. There are higher order effects in the ladder terms of the polarization expansion but will not be discussed do to the scope of this research.

As shown in the polarization expansion the refractive index of some materials has a dependence on the incident irradiance, high irradiance levels result in a change in index. This nonlinear behavior is referred to as the Kerr or bound electronic effect. Nonlinear refraction (NLR) is an effect resulting from high intensity levels in the  $\text{GW}/\text{cm}^2$  regime interacting with a material and comes from the real part of the third order nonlinear susceptibility. Another term that is present in semiconductor materials is called the free carrier refraction coefficient ( $\sigma_f$ ). One can think of the free carrier refraction coefficient as the number of free carriers that interact with a laser beam per unit volume. These free carriers are generated from linear absorption in the material and they affect the way light is refracted.

Much like NLR, the amount of light a material absorbs is dependent on the magnitude of incident irradiance; this dependence is called nonlinear absorption (NLA). The lowest order physical mechanism that is responsible for this nonlinear behavior is two photon absorption ( $\beta$ ), a process whereby two photons are simultaneously absorbed in the medium, exciting an electron from the valence band into the conduction band as seen in Fig. 2.1.

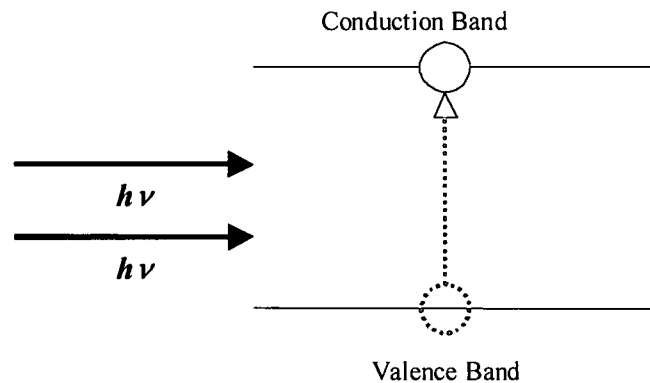


**Fig. 2.1: Two photon absorption process**

Two photon absorption is a third order nonlinear process; specifically, it comes from the imaginary part of the third order susceptibility. Depending on the pulse duration the material under test can have free carrier absorption present. This term can be thought of as the number of free carriers that interact with the laser beam per unit area. These free carriers are created from the high intensity levels and affect the way light is absorbed in the material.

## **2.2 Different Measurement Methods**

There are various measurement techniques that can be employed to determine the optical nonlinearities of a material. Some of these methods include, but are not limited to, various z-scan techniques, nonlinear

interferometry, and irradiance scans. All of the techniques mentioned have their strengths and limitations depending on the specific application in which they are used. Optical nonlinearities have also been calculated using mathematical modeling methods. Below, each of the above mentioned techniques will be discussed briefly, including a description of the application, strengths, weaknesses, and problems that arise using each method.

Many mathematical models have been constructed to theoretically calculate the value of NLR and NLA terms. Once these mathematical models have been developed, one can run a computer simulation to find out the optical nonlinearities of the material of interest in a matter of minutes. Modeling these properties at various temperatures is simpler than actually conducting an experiment to measure them. When compared to other techniques, modeling can be less accurate but it is useful for estimating  $\gamma$ ,  $\sigma_r$ ,  $\beta$ , and  $\sigma_a$ .

The z-scan<sup>1,2</sup> technique is a widely used method for determining the nonlinear optical properties of materials. Past z-scan experiments have determined the optical nonlinearities of solid and liquid materials. In this method the sample is translated through the focus of a beam that has a known temporal and spatial profile. A detector placed in the far field monitors the energy transmitted through the sample as a function of sample position. When a sample with  $\gamma < 0$  is placed before the focus and then translated toward focus, the far field beam starts to collimate due to a positive lensing effect (see Fig. 2.2). The dashed lines indicate how the beam would propagate if the material with the

nonlinear index of refraction were not present and the solid show what actually happens.

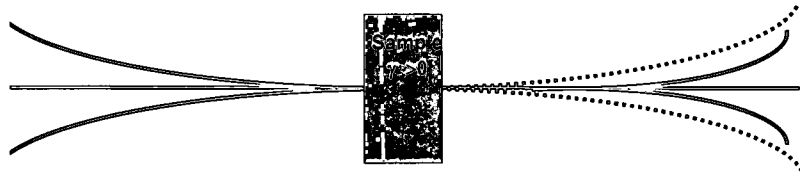


**Fig. 2.2: Diagram of negative lensing effect**

The exact opposite results for samples with a positive  $\gamma$ . The z-scan method has become somewhat of a standard measurement technique due to the ease of finding the magnitude and sign of  $\gamma$ . The pointing of the beam is crucial, and the spatial quality of the beam must be excellent in the experimental setup due to the fact that the sample is moving through focus. Since most analyses take the thin film approximation the sample thickness must be small relative to the Rayleigh range of the experimental setup. A Rayleigh range is defined as the distance along the axis a beam is propagating from the waist to point at which the cross section doubles.

Keeping the Rayleigh range large with respect to the sample thickness can prove to be difficult due to hardware constraints when translating the sample. Usually translation stages are only a few centimeters long and the sample needs to be translated through multiple Rayleigh ranges. As a result, the sample thickness is only one or two orders of magnitude smaller than the Rayleigh range, so the validity of the thin sample approximation is compromised. Another

problem when using this method is that it is difficult to distinguish between variations in transmission due to sample imperfections and sample nonlinearities.

Imaging Z-Scan<sup>3</sup> method where the input beam is no longer a Gaussian profile but has a circular flat top. This method allows more distinction between the peak and valley of the transmission profile as a function of  $z$ , and thus more sensitivity. Having a more distinct transmission profile allows post-process curve fitting to be done with greater accuracy. However the same drawbacks apply to this technique as do the original z-scan.

Two dimensional Z-scans<sup>4</sup> use a Charge Coupled Device (CCD) for the detector, which provides multiple advantages over a photodiode detection system. When a CCD is used there is an added advantage that the image can be stored and analyzed later. The size of the array is also large enough to allow the experimenter to monitor the reference and the far-field beam profile simultaneously. This allows the experimenter to normalize fluctuations in the beam shape. These fluctuations during the experiment affect the refractive index, which complicates the analysis of the z-scan data. Accurate pictures of the beam profile are possible because CCD technologies have progressed to the point where pixel sizes are on the order of  $1\text{ }\mu\text{m}$ . Usually the spot size at focus is a few orders of magnitude larger than the pixel size. CCD technologies have a large dynamic range, allowing the experimenter to drastically vary the intensity level on the device without affecting the linearity. The array of the CCD is also much larger than other detectors, so the whole far-field distribution pattern can be captured. One of the limitations of this method is that CCD cameras only

have a linear response over a narrow spectrum, depending on the material from which the sensor is constructed. CCD technologies are improving but currently this can limit the wavelengths at which two dimensional z-scans can be used for nonlinear optical property characterization applications.

Another method that is used for finding NLA and NLR terms is an interferometric technique<sup>5</sup>. This technique usually uses a Mach-Zehnder interferometer where outputs from both arms of the interferometer are carefully overlapped temporally and spatially and focused on a high resolution camera. The material under test is inserted in one arm of the interferometer and a material with a known nonlinearity and an equivalent optical path length is inserted into the other arm. The intensity and phase are varied between the two arms. The two arms of the interferometer combine to form an interference pattern at the output. When the interference pattern is no longer dependent on intensity the linear path lengths of the arms are equal and the nonlinear path length increases. The ratio of intensities of both arms of the interferometer is inversely proportional to the ratio of the NLR of both arms of the interferometer; this is how the NLR coefficients are found. A drawback of this method is that the alignment of the interferometer is complicated yet crucial for reliable results, and the quality of the beam must be excellent.

The final experimental method to be discussed will be the intensity scan method<sup>6</sup>, commonly referred to as the I-scan. The basic set up of this technique starts out with some means of attenuating an optical pulse, followed by optics to focus the light onto the sample. The sample under test is placed slightly before

focus. As the pulse intensity is varied a reference detector monitors the incident intensity and laser energy fluctuations. A closed aperture detector placed in the near field monitors the on-axis fluence transmitted through the sample as a function of the pulse intensity. A second detector monitors the total transmitted energy through the sample. This method has an advantage over the methods described earlier because the sample is not translated through focus. As a result, the sample is not moving through the focal plane where it would be exposed to large irradiance levels which may damage the sample. When the sample is placed before focus there are positional dependences such as the radius of curvature, beam radius, and the sample position.

There are many more techniques currently being utilized to determine the optical nonlinearities of materials. All of the methods mentioned were considered when designing the experimental method that was ultimately used. Given the project goals and limitations, one of the methods was optimized to measure the temperature dependent optical nonlinearities of semiconductors.

### ***2.3 Research Goals and Experimental Considerations***

As we have seen, there are a number of techniques capable of measuring the two photon absorption coefficient and nonlinear index of refraction. The goal of this experiment is to measure  $\gamma$ ,  $\sigma_r$ , and  $\beta$  for a semiconductor material at both room and cryogenic temperatures. The chosen experimental design had to meet these goals while also accounting for practical considerations.

Finding the optical nonlinearities across a temperature range provides a major challenge. Since operating at low temperatures in atmosphere would



result in condensation on the samples, the sample must be placed in a dewar at vacuum. Adjustments to the sample position in the dewar are not possible once a vacuum is created. The use of a dewar also introduces two more optics into the experimental system, since it must include front and rear windows to transmit the optical pulse. If vacuum is broken while the dewar is full of liquid nitrogen the temperature differential will not only cause condensation on the sample but on both windows. Condensation can affect transmission and reflection properties of the surfaces.

The dewar is of substantial size and the cryostat has associated vacuum and electrical lines (see Fig. 2.3). Measuring temperature dependencies where a cryostat and dewar are required proves to be difficult especially when the associated hardware is required to move in a sensitive optical setup.

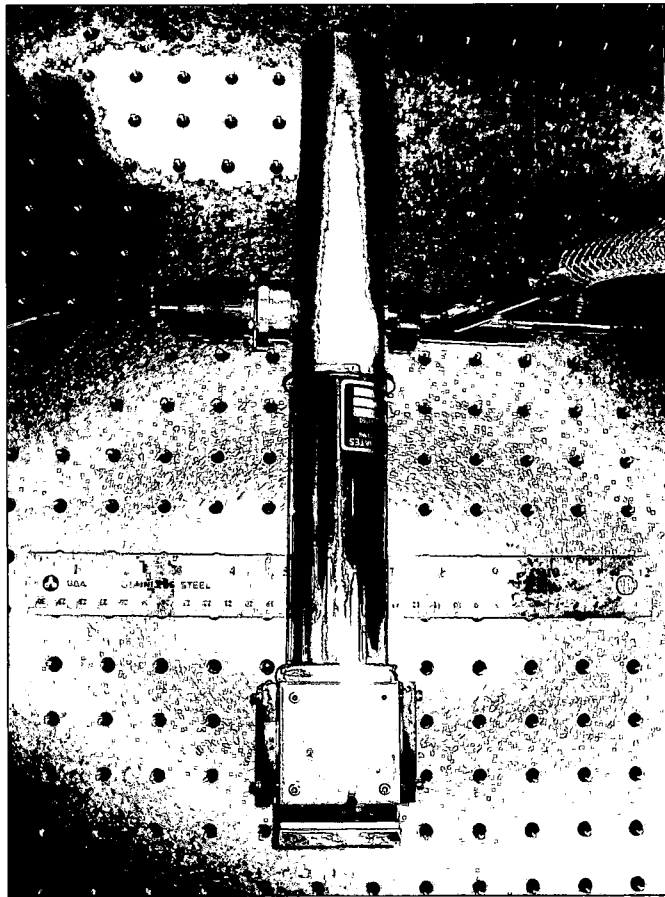


**Fig. 2.3: Cryostat, dewar, and required electrical/vacuum lines**

The experiment had to be conducted in a manner in which no damage was inflicted on the sample under test. The sample itself presented another limitation. The samples studied in this project are thin pieces of semiconductor material that are prone to damage and may only have a fraction of a square centimeter available from which to pick a test site. When a sample is translated through focus problems arise from the change in beam pointing which occurs when the sample is translated. As the pointing changes, the beam can walk off the active area of fixed detectors. Fig. 2.4 is an illustration of a beam walking off the active area of a detector as a wedged material is translated.

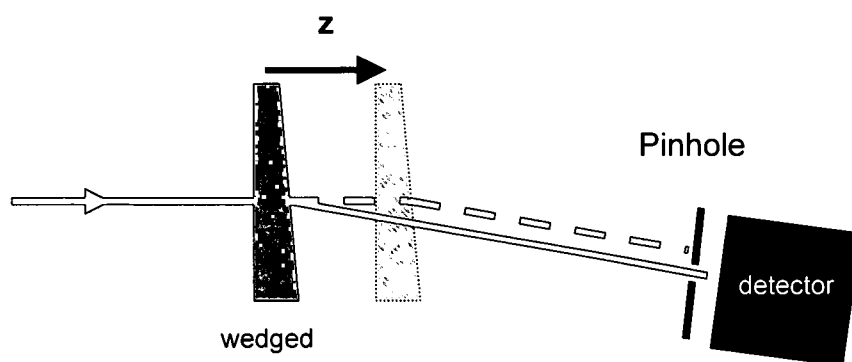


**Fig. 2.4: Beam walking Illustration**

The magnitude of the irradiance on the detection system is going to change substantially during the experiment. The detection system needs to have a linear response to the change in intensity. Small nonlinearities will be measured on this system; in order to do this, the detectors used need to have minimal noise and good linearity at  $1.064\mu\text{m}$  wavelength.

Looking at the project goals and the associated hardware restrictions a technique was developed to measure the temperature dependent optical nonlinearities of semiconductors.

## **2.4 Experimental Method**

As we have seen, translating wedged samples introduces problems with beam walk-off. Further, translation of the setup at cryogenic temperatures can be unwieldy. Ideally, one would leave the sample fixed and vary instead the incident energy, which would eliminate these concerns. For this reason, a modification of the intensity scan technique was chosen to be used, together with a modified analysis routine. By using the intensity scan technique we were able to eliminate issues created when a wedged sample is translated through focus as in a z-scan (Fig. 2.5).

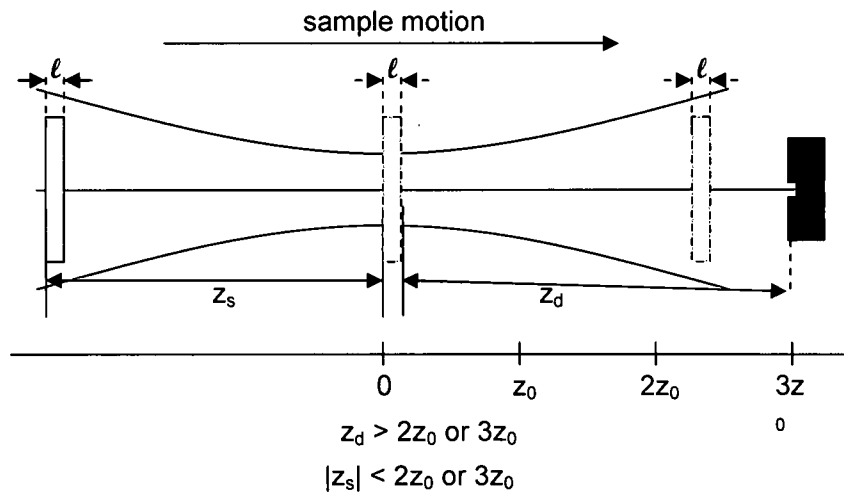


Fig. 2.5: Z-Scan optical schematic

By using a modification of the intensity scan technique (Fig. 2.6) the distance from the sample to the detection system was constant. By keeping the separation constant, the pointing caused from wedged materials could be accounted for one time when the sample was placed in the system.

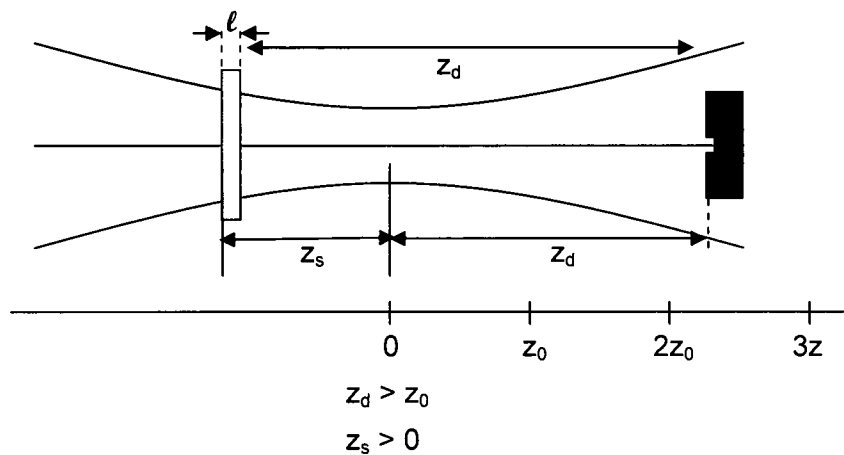
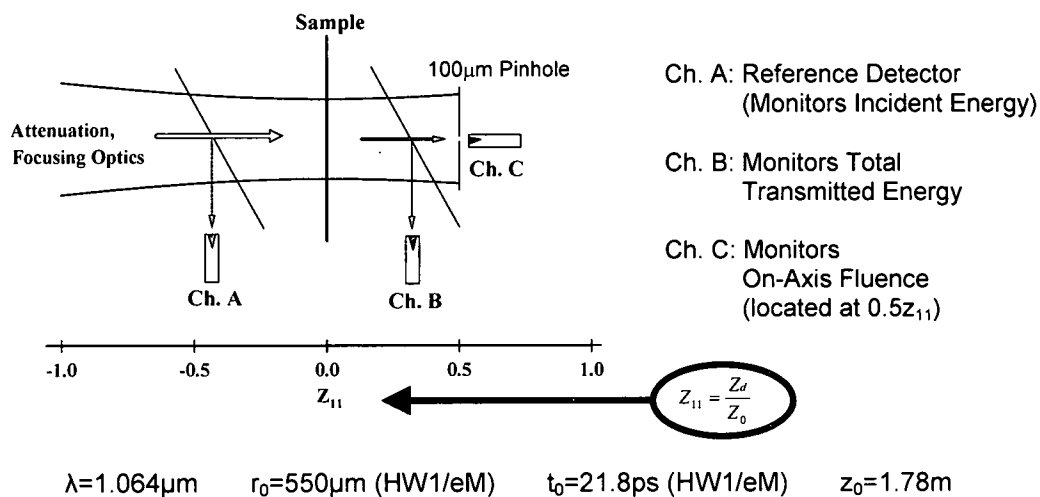


Fig. 2.6: I-Scan optical schematic

In past z-scan and l-scan experiments, the closed aperture detector has been placed in the far field and the sample was fixed ahead of focus in the l-scan method. The sample and detector were positioned differently in this research: the closed aperture detector is located in the near field and the sample is fixed at focus. For this experiment the sample was fixed at focus, and the detector was placed in the near field at  $z_{11} = 0.5$ , where

$$z_{11} \equiv \frac{\text{Sample to Detector Separation}}{\text{Rayleigh Range}} \equiv \frac{z_d}{z_0} \quad (2.3)$$

The optimized test bed used in this experimentation is shown in Fig. 2.7.



**Fig. 2.7: Optical test bed designed and implemented**

A wave plate followed by a Glan Thompson polarizer is used to variably attenuate the pulse from a 1.064  $\mu\text{m}$  Nd:YAG picosecond laser. Optics are used to weakly focus the beam onto the sample fixed at focus. A pick-off is placed in front of the sample to monitor the incident laser irradiance and monitor any drift

or fluctuations from the laser. The sample under test is mounted on a cryostat that is placed inside a dewar; the entire apparatus remains fixed. Following this assembly, another pick-off is used to send portions of the transmitted pulse to closed and open aperture detectors.

The closed aperture detector is placed half of a Rayleigh range from the back face of the sample to monitor the on-axis fluence through the sample. The open aperture detector monitors the total transmitted energy through the sample. With a sample in place the pulse is variably attenuated while the signals on all three detectors are acquired simultaneously and captured in a LabVIEW routine. In order to calibrate each channel, the measurement is repeated with the sample removed. Absolute transmission values are obtained by normalizing the sample data channels to the calibration data.

Deriving the values of the nonlinear optical parameters  $\gamma$ ,  $\sigma_r$ , and  $\beta$  from the experimental data requires a theoretical model. The model must of course involve measurable quantities (namely,  $T_e$  and  $T_f$ ). The details of the model used in this work are discussed in the chapter which follows.

## Chapter 3

### Irradiance Scan Theory

#### 3.1 *Nonlinear Beam Propagation in a Semiconductor*

The preceding chapter discussed in detail the data acquisition method. How does one determine the nonlinear optical parameters from the acquired data? Doing so requires a model for light propagation through a semiconductor.

The relationship<sup>1</sup> between the irradiance of light incident upon a semiconductor and absorption in the material is given by

$$\frac{\partial I}{\partial z} = -\alpha I - \beta I^2 - \sigma_a N I \quad (3.1)$$

where Irradiance ( $I$ ), propagation distance ( $z$ ), free carrier density ( $N$ ), and other quantities are as discussed in Chapter 2. The free carrier density is the number of free charge carriers per unit volume. The rate of change in the free carrier density depends on single photon absorption, two photon absorption, and the carrier lifetime:

$$\frac{\partial N}{\partial t} = \frac{\alpha I \lambda}{hc} + \frac{\beta I^2 \lambda}{2hc} - \frac{N}{\tau_d} \quad (3.2)$$

Here,  $(h)$  is Plank's constant,  $(c)$  is the speed of light, and  $(\tau_d)$  is the free carrier lifetime. The final partial differential equation, given by Eqn. 3.3, models the rate of change in phase through the sample.

$$\frac{\partial \phi}{\partial z} = \frac{2\pi}{\lambda} (\sigma_r N + \mathcal{H}(\phi)) \quad (3.3)$$

Particular aspects of the experimental setup permit further simplifications, as discussed below.

### **3.2 Analysis Assumptions**

At low repetition rates and short pulse durations any photo-excited free carriers will have an infinite lifetime. For short wave infrared wavelengths, charge carrier lifetimes are typically in the tens of nanoseconds. For picosecond pulses as are used in these experiments, any accumulated free carriers will have decayed long before the next pulse arrives, so each pulse is independent of the preceding. Additionally, it can be safely assumed that no thermal effects are contributed from the laser, again owing to the low total energy in the short laser pulse.

The solutions to Eqns. 3.1 through 3.3 assume an input beam that has a Gaussian profile in both space and time. The beam is assumed to have a flat phase front at the first face of the sample, which is why the sample was placed at focus. The model neglects diffraction within the sample, which is equivalent to the thin sample approximation. The thin sample approximation is valid because the sample thickness is several orders of magnitude smaller than the Rayleigh range of the test bed.



With the assumptions discussed above, partial differential equations (3.1), (3.2), and (3.3) reduce to

$$\frac{\partial I}{\partial z} = -\alpha I - \beta I^2 + \sigma_a NI \quad (3.4)$$

$$\frac{\partial N}{\partial t} = \frac{\alpha I \lambda}{hc} + \frac{\beta I^2 \lambda}{2hc} \quad (3.5)$$

$$\frac{\partial \phi}{\partial z} = \frac{2\pi}{\lambda} (\sigma_r N + \gamma I) \quad (3.3)$$

The nonlinear optical coefficients are determined by simultaneously solving three simplified partial differential equations, assuming an input beam with the same spatial and temporal profiles as the physical beam.

### 3.3 Determining $\beta$

The two photon absorption coefficient is found by fitting the total energy transmission to 3.7<sup>7</sup>.

$$T_E = \frac{2}{Q\sqrt{\pi}} (1-R) e^{-\alpha l} \int_0^\infty \ln(1 + Q e^{-x^2}) dx \quad (3.7)$$

where  $Q = \beta(1-R)I_0 \left( \frac{1 - e^{-\alpha l}}{\alpha} \right)$

The only free variable in (3.7) is the two photon absorption coefficient. A computer algorithm varies the value of the two photon absorption coefficient in (3.7) until the best fit is found.

### 3.4 Determining $\gamma$ and $\sigma_r$

Using the on axis fluence data, the value of  $\beta$  from the previous step, and other known parameters, the nonlinear index of refraction and the free carrier

refraction coefficient are found. The nonlinear beam propagation calculation takes place in two steps, corresponding to the two regions illustrated in Fig. 3.1.

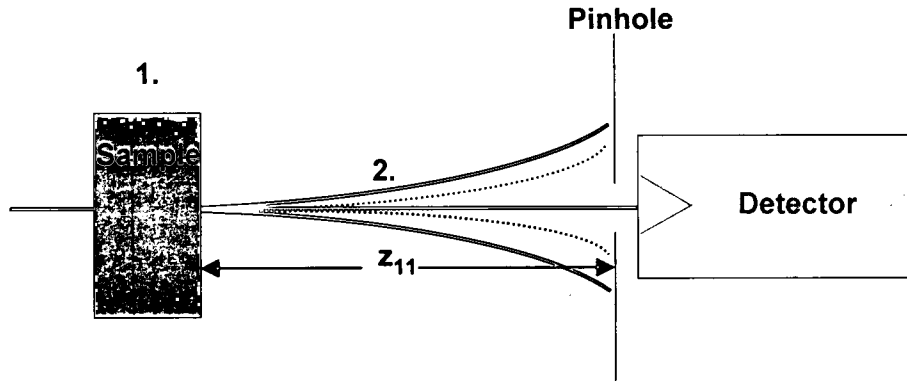


**Fig. 3.1: Nonlinear beam propagation schematic ( $\gamma < 0$  shown)**

In the first step, the beam is propagated from the front face of the sample to the back face. The electric field profile at the front face of the sample is known from a careful beam profile measurement. The values of some material parameters are known from previous experiments. One parameter ( $\beta$ ) is known from the previous step, and the remaining parameters ( $\gamma$ ,  $\sigma_r$ , and  $\sigma_a$ ) are provided with initial guesses. A finite difference method is employed to propagate the beam through the sample; at each step, by solving partial differential equations (3.4), (3.5), and (3.6).

Having propagated the beam through the sample, it remains to the second step to propagate the beam to the closed aperture detector, a normalized distance  $z_{11}$  away. The field distribution is calculated using the Huygens-Fresnel diffraction formalism. To determine the on-axis fluence transmission at the detector, the on-axis fluence at  $z_{11}$  is simply divided by the same quantity in the absence of the sample. In this manner, the electric field profile for an initial

guess of  $\gamma$ , and  $\sigma_r$  is calculated at varying input irradiances. For each input irradiance value, the magnitude of the on-axis electric field is squared and integrated with respect to time, yielding a quantity proportional to the on-axis fluence<sup>B</sup>. Hence for a given  $\gamma$  and  $\sigma_r$ , an on-axis fluence transmission is calculated. A mean square error between this calculated curve and the experimental curve determines the fitness of the  $(\gamma, \sigma_r)$  pair. The parameters  $\gamma$  and  $\sigma_r$  are varied until the least mean square error is found. The parameters yielding the least mean square error are the material parameters.

Using this finite difference approach as well as curve fitting, the nonlinear optical properties of three semiconductors were found at room and cryogenic temperatures. The following chapter will discuss the three semiconductors that were characterized in this research.

---

<sup>B</sup> The fluence of course is energy per unit area, so two additional factors are required, but these cancel when the fluence is divided by the fluence in the absence of the sample.

## **Chapter 4**

### **Overview of Materials Characterized**

#### ***4.1 Materials Selected For Characterization***

The nonlinear optical properties of three semiconductor materials were characterized at room and cryogenic temperatures using the irradiance scan method. A number of factors went into the choice of the materials to test. It was important to choose materials that would be of interest at the 1.064  $\mu\text{m}$  wavelength. The materials selected needed to verify that the irradiance scan method was working correctly so some of the materials' nonlinear optical properties needed to have been previously measured using proven techniques. This gave us the ability to verify that the irradiance scan measurement technique was yielding the correct nonlinear optical coefficients.

Carbon disulfide ( $\text{CS}_2$ ) was used as a calibration sample to verify that the experimental setup and data analysis yielded the expected results. Gallium Arsenide (GaAs), Indium Phosphide (InP), and Cadmium Telluride (CdTe) were selected as the semiconductors to be characterized at room and cryogenic temperatures.

## **4.2 Material Applications & Overview**

$\text{CS}_2$  is of limited use in optical applications, but owing to its well characterized nonlinear index of refraction it is used here as a benchmark. It is important to know the nonlinear optical properties of a material such as  $\text{CS}_2$  for comparison purposes, as without this calibration material, the nonlinearities of other materials could not be measured with confidence.

GaAs is a direct band gap semiconductor with high electron mobility, and a cubic symmetry. It has been noted<sup>2</sup> that GaAs has nonlinear optical characteristics that allow it to function well as an optical power filter. An optical power filter makes use of a material's nonlinear optical properties to reduce the optical transmission; both nonlinear refraction and nonlinear absorption contribute to this behavior. The plot of total energy transmission through the sample as a function of incident irradiance approaches a horizontal asymptote as irradiance increases, similar in shape to the I-V curve of a Zener diode. Just as a Zener diode is used for over voltage protection, an optical power filter can be used to attenuate high irradiance levels that may damage a device. Large samples of GaAs with variable electrical parameters are now available due to technical advances.

Texas Instruments<sup>8</sup> (TI) has developed economical manufacturing techniques that allow GaAs to be grown with surface areas on the order of square feet. TI has also created a method of producing GaAs with high and low impedances with material ruggedness such that it will hold up in physically harsh

environments. High impedance GaAs is useful for optical power filter applications, high speed windows, prisms, and lenses. Low impedance GaAs is useful in electrical applications such as limiting electromagnetic induction filter. Manufacturers can variably tune the impedance of GaAs allowing a filter to be produced that only transmits certain optical and electrical signals. With these new manufacturing innovations, GaAs is a prime candidate for use in both optical and electrical filters. GaAs is used in high efficiency solar cells; the highest efficiency solar cells are made out of a combination of Ga and InP.

InP is another direct band gap semiconductor that is used in solar cell applications that require high efficiencies. InP is also used in optical integrated circuit applications<sup>9</sup>. The advantages of using optical integrated circuits over conventional optics include a dramatic reduction in size, the elimination of any alignment, and a substantially reduced cost. Manufacturing processes that were developed and refined by the computer industry are used to make optical amplifiers, waveguides, modulators, and gratings on a single small chip. InP modulators built in integrated circuits have excellent switching rates that the telecommunications industry utilizes. Other applications of InP include optical power filters and multiple detector technologies. Gratings are constructed of InP for tunable semiconductor lasers; this is accomplished by layering *n*- and *p*- type InP.

The final semiconductor selected for characterization, CdTe, shares applications with both GaAs and InP. CdTe and other semiconductors are used in the construction of diode lasers because the output coupler can be constructed

easily. When semiconductors are deliberately scratched and a small force is applied, a perfect mirror-like cleave is formed where the material breaks. CdTe works well for laser manufacturing, optical quality IR windows, photovoltaic cells, and electro-optic modulators. CdTe is an excellent electro-optic modulator because it has the highest electro-optic coefficient of Type II-VI crystal structures.

CdTe is used as a photoconductive layer in photovoltaic cells<sup>10</sup>, because its transmission spectrum closely matches the sun's spectrum. When CdTe is sandwiched in-between a material such as cadmium sulfide, the combination forms the *p-n* junction required to make a photovoltaic cell.

GaAs, InP, and CdTe clearly share similar applications; some applications such as gratings, detectors, and e-o modulators<sup>11</sup> actually involve compounds of the materials. In order to develop new compounds it is important to understand all of the properties of the individual materials. Scientists and engineers have put significant effort into characterizing the material properties of GaAs, InP, and CdTe. Characterization results relevant to the scope of this research will be presented next.

### **4.3 *Material Characterization Values from Literature***

CS<sub>2</sub> optical nonlinearities have been measured in the past using multiple measurement methods. Past experiments<sup>12</sup> using 1.064  $\mu\text{m}$  wavelength light indicate that the only non-zero optical nonlinearity in CS<sub>2</sub> is  $\gamma$ , as shown in Table 4.1. (These measurements were performed at 300 K.)

**Table 4.1: Previously measured CS<sub>2</sub> NLR & NLA coefficients**

		$\gamma$ ( $10^{-14}$ cm <sup>2</sup> /W)	$\sigma_r$ ( $10^{-21}$ cm <sup>3</sup> )	$\beta$ (cm/GW)
Sample	T(K)	Prior <sup>12</sup>	Prior	Prior
CS <sub>2</sub>	300	3.1	-	-

GaAs, CdTe, and InP have been studied and used in optical applications for many years now, and as a result, the optical properties of these semiconductors are well-characterized. Depending on the material, temperature range, and wavelength used, different levels of investigation have been conducted on these semiconductors. Specifically, the nonlinear optical coefficients  $\gamma$ ,  $\sigma_r$ , and  $\beta$  that have been previously measured at 1.064  $\mu$ m for GaAs, CdTe and InP will be presented.

For GaAs, the nonlinear index of refraction, free carrier refraction coefficient and two photon absorption coefficient have been measured at room temperature. The measurements<sup>13</sup> that will be used as a reference for this research were done with the z-scan technique, and the results are shown in Table 4.2.

InP NLA and NLR values have been measured at room temperature. The measurements<sup>14</sup> that were chosen as a reference for this research were done with the z-scan technique, and the results are shown in Table 4.2.

Likewise, the nonlinear index of refraction, free carrier refraction coefficient, and two photon absorption coefficient for CdTe have been measured at room temperature. The measurements<sup>13</sup> cited here were also performed with the z-scan technique (Table 4.2).



**Table 4.2: Previously measured GaAs, InP, and CdTe NLR & NLA coefficients**

		$\gamma$ ( $10^{-14}$ cm <sup>2</sup> /W)	$\sigma_r$ ( $10^{-21}$ cm <sup>3</sup> )	$\beta$ (cm/GW)
Sample	T(K)	Prior	Prior	Prior
GaAs	300	-41 <sup>13</sup> & -150 <sup>14</sup>	-5.9 <sup>13</sup> & -0.4 <sup>14</sup>	26 <sup>13</sup> & 35 <sup>14</sup>
GaAs	77	-	-	-
InP	300	-150 <sup>14</sup>	-0.4 <sup>14</sup>	90 <sup>14</sup>
InP	77	-	-	-
CdTe	300	-27 <sup>13</sup>	-5.2 <sup>13</sup>	26.1 <sup>13</sup>
CdTe	77	-	-	-

All of the semiconductors room temperature nonlinear optical properties were measured at 1.064  $\mu$ m using a z-scan method. Having the ability to compare the irradiance scan method's results to past measurements allowed us to verify that the method produced reasonable results before moving on and measuring previously uncharacterized optical properties.

#### **4.4 Uncharacterized Optical Properties**

To our knowledge, the temperature dependence of the optical nonlinearities of GaAs, InP, and CdTe at 1.064  $\mu$ m has not been previously examined experimentally. When a semiconductor experiences a change in temperature, the band gap energy changes which, in turn, leads to a change in the optical nonlinearities. For example, the two-photon absorption coefficient is related to the band gap energy shown in equation 4.1<sup>13</sup>.

$$\beta(\omega) = K_{ph} \frac{\sqrt{E_p}}{n_0^2(\omega) E_g^3} F_2 \left( \frac{h(\omega)}{E_g} \right)$$

$$\text{where } F_2 = \frac{(2x-1)^{3/2}}{(2x)^5} \quad (4.1)$$

$$K_{ph} = \frac{2^9 \pi}{5} \frac{e^4}{\sqrt{m_0 c^2}}$$

Here  $E_p$  is the photon energy,  $E_g$  is the band gap energy,  $n_0$  is the linear refractive index, and  $m_0$  is the electron mass. The two photon absorption coefficient is a function of band gap energy, so it is expected that  $\beta$  should change with temperature. Using Eqn. 4.1,  $\beta$  was calculated for each of the three semiconductors at both 300 K and 77 K.

In addition, another, more accurate method (employing the full band structure of InP) was used to determine  $\beta^{15}$ . The theoretical value found using this method is higher by ~35% than what was determined using Eqn. 4.1. In this research the theoretical  $\beta$  value using the full band structure will be used for comparison with the measured values of InP. Since theoretical values using the full band structure were not available for GaAs and CdTe,  $\beta$  values using Egn. 4.1 will be used for comparison for these two semiconductors. The results are tabulated in Table 4.3.

**Table 4.3: Theoretical  $\beta$  for GaAs, InP, and CdTe at 300 K and 77 K**

Sample	$\beta$ (cm/GW) Theoretical T=300 K	$\beta$ (cm/GW) Theoretical T =77 K
GaAs	17.6 <sup>13</sup>	15.7 <sup>13</sup>
InP	17.3 <sup>13</sup> 23.4 <sup>15</sup>	15.5 <sup>13</sup> 21.1 <sup>15</sup>
CdTe	25.1 <sup>13</sup>	21.1 <sup>13</sup>

The calculated theoretical two photon absorption coefficient is ~12% smaller for all three semiconductors when the temperature is decreased from 300 K to 77 K. To the best of our knowledge this was the first time an irradiance scan has been used to measure optical nonlinearities of semiconductors. We also believe this was the first time temperature dependent optical nonlinearities have been measured for GaAs, InP, and CdTe. The experimental results will be presented in the chapter to follow.

## Chapter 5

### Results

#### **5.1 *Definition of Error in Measurements***

In this chapter, the measured  $\beta$ ,  $\gamma$ , and  $\sigma_r$  values will be presented for CS<sub>2</sub> and three semiconductors (GaAs, InP, and CdTe) measured at both 300 K and 77 K. Transmission spectra for each material will be presented along with fits to the data used in the determination of the optical nonlinearities. Once all of the optical nonlinearities were determined, all of the parameters were varied individually until the uncertainty of each measurement was found.

The uncertainty of the measurement of all the values presented in this chapter was defined as the change in the fitted value necessary to yield a 7.5% change in the RMS error. The process for determining the error in the fit was relatively straight forward. For the parameter being fit, different values were plugged into the model and the RMS error with respect to the experimental curve was recorded. A quadratic function was fit to these RMS values, and using that quadratic fit, the corresponding value for a 7.5% change in RMS error was determined. Finally, the error in the measurement is found by comparing the parameter value having minimum RMS error to the parameter value with a 7.5% change in RMS error. This method of determining the uncertainty of the measurement was used for all quantities presented in this chapter.

## 5.2 *Verification of Test Bed's Accuracy*

If this measurement system was to be used to determine unknown  $\beta$ ,  $\gamma$ , and  $\sigma_r$  of materials we needed to be confident that the method was indeed working correctly. The method used for determining  $\beta$  has been proven in the past in our laboratory<sup>16</sup> as well as others, so no further verification was required. The system's ability to measure  $\gamma$ , and  $\sigma_r$  in the absence of  $\beta$  had not been tested. Furthermore, we wanted to measure  $\gamma$  in the absence of any  $\sigma_a$ , and  $\sigma_r$ , so as to reduce the complication of the fit / test, and see if  $\gamma$  can be measured accurately when no other nonlinear effects are present. A natural test candidate to verify this functionality is CS<sub>2</sub>.

The first sample to be tested using the irradiance scan method was a 25mm cell of carbon disulfide (CS<sub>2</sub>). CS<sub>2</sub>'s nonlinear index of refraction has been measured on various experimental setup configurations, making it a good material candidate for calibration purposes. CS<sub>2</sub> does not have nonlinear absorption or free carrier absorption/refraction effects. This not only simplified the analysis of the data but allowed us to test the method's ability to fit the nonlinear index of refraction without relying on the correctness of the two photon absorption coefficient determined from that fit.

With the closed aperture detector at  $z_{11}=0.5$ , the data shown in Fig. 5.1 was found.

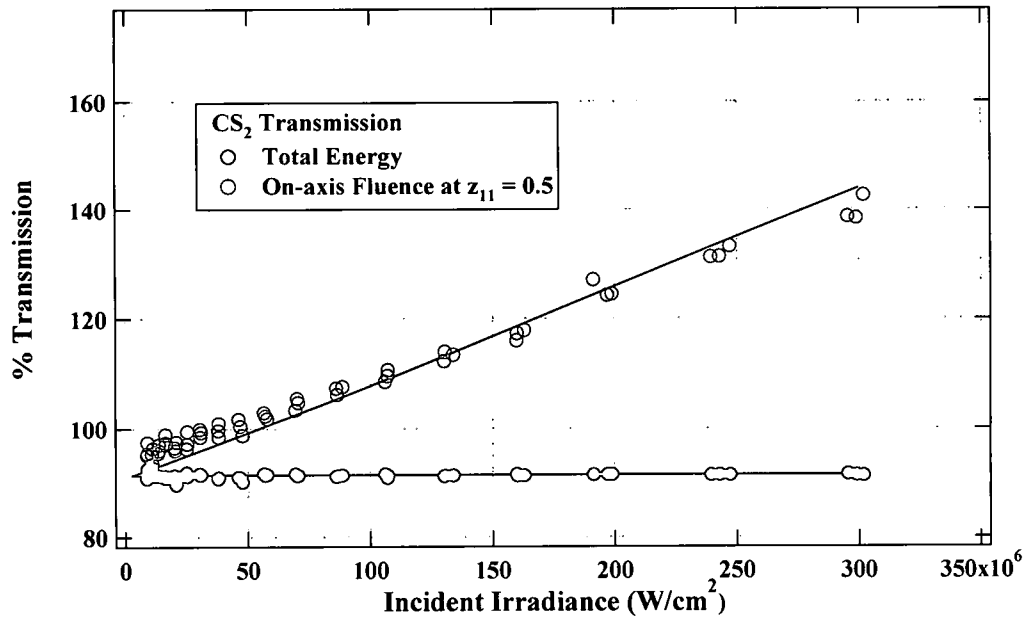


Fig. 5.1: CS<sub>2</sub> NLA, and NLR at 300 K

Using the computer algorithm, a line representing the best fit of the data was generated. The total energy transmittance (open aperture) fit is a horizontal line, indicating the absence of two photon absorption in the CS<sub>2</sub> sample. The nonlinear index of refraction was determined with another computer algorithm using the on-axis fluence transmission data (closed aperture). Both the nonlinear absorption and refraction values for CS<sub>2</sub> measured in this research are in agreement with previous results. The previously measured  $\gamma$  for CS<sub>2</sub> falls within the 4% uncertainty of our measurement. The tabulated values are shown in Table 5.1.

Table 5.1: CS<sub>2</sub> measured NLR

				$\gamma$ ( $10^{-14}$ cm <sup>2</sup> /W)		$\sigma_r$ ( $10^{-21}$ cm <sup>3</sup> )		$\beta$ (cm/GW)	
Sample	T(K)	Thickness (mm)	$\sigma_a$ Used	This Work	Prior	This Work	Prior	This Work	Prior
CS <sub>2</sub>	300	25	-	3 $\pm$ 4%	3.11 <sup>12</sup>	-	-	-	-

This agreement, particularly since it involves even a small nonlinear index of refraction, instills confidence in the values obtained using this technique. We were able to move forward and measure the optical nonlinearities for materials with nonzero nonlinear absorption and free carrier refraction with confidence.

### 5.3 Measured NLA & NLR of GaAs

The nonlinear optical properties of three semiconductors were characterized using the irradiance scan technique at both 300 K and 77 K. The first semiconductor that was characterized was a 0.42 mm thick sample of GaAs. Spectra were taken of the GaAs sample at both 300 K and 77 K and are shown in Fig. 5.2.

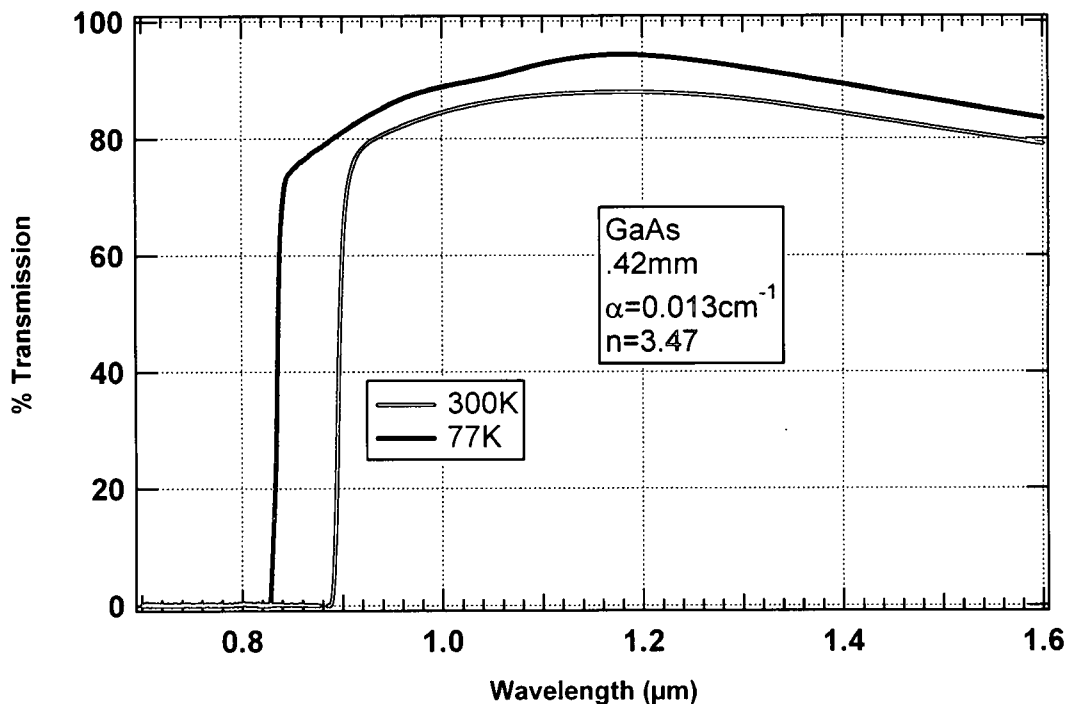
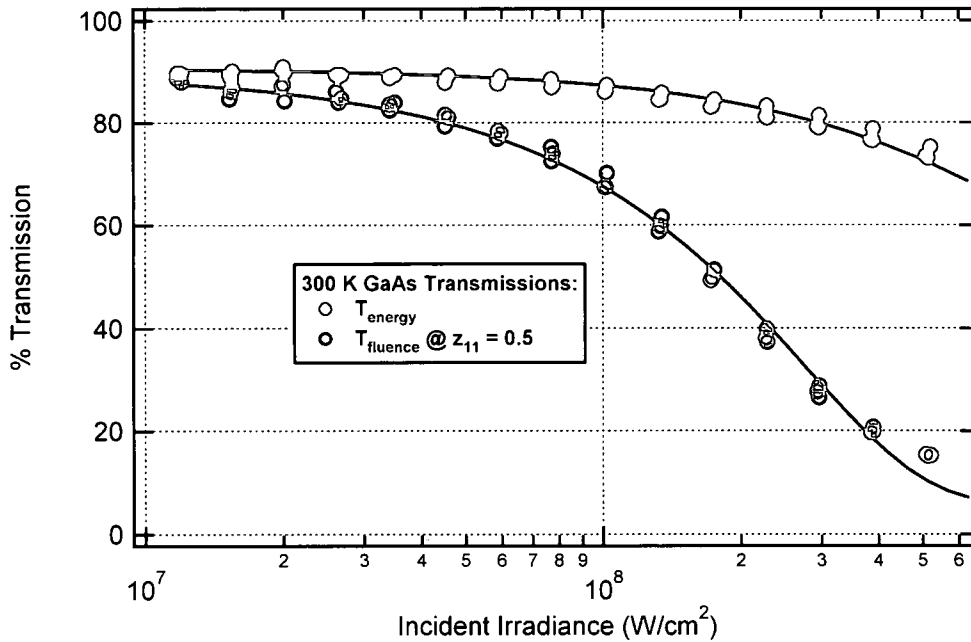


Fig. 5.2: GaAs spectra at 300 K and 77 K

The band gap energy of GaAs clearly illustrates a dependence on temperature, so it was expected (Egn. 4.1) that different two photon absorption coefficients

would be measured at 77 K and 300 K. The only material tested in this research where the effects of free carrier absorption were observed was GaAs. For the data analysis of GaAs, a  $\sigma_a$  value of  $5 \times 10^{-17} \text{ cm}^3$  from the literature<sup>17</sup> was used, using this  $\sigma_a$  value the fits shown in Fig. 5.3 were made at 300 K. The closed aperture detector that monitors the on-axis fluence was located at  $z_{11} = 0.5$ .



**Fig. 5.3: GaAs NLA, and NLR at 300 K**

The measured nonlinear absorption and refraction terms at 300 K for GaAs are shown in Table 5.2. Data was then collected for the GaAs sample at 77 K. Plots of the results and best fits are shown in Fig. 5.4.



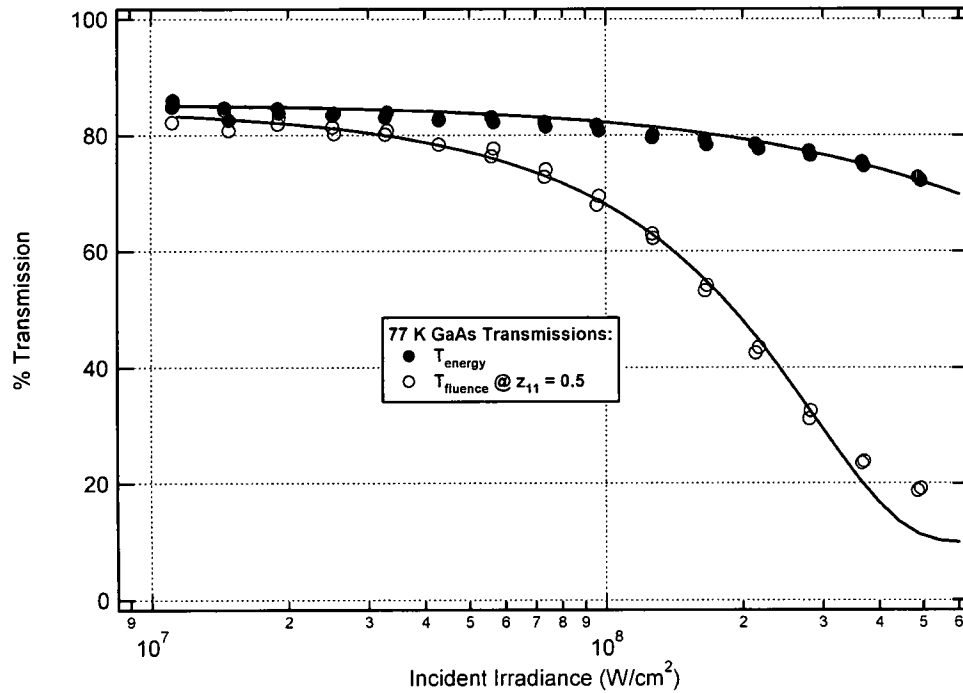


Fig. 5.4: GaAs NLA, and NLR at 77 K

The nonlinear absorption and refraction terms and the uncertainty of the fitted value at 77 K are summarized in Table 5.2 along with past experimental results and theoretical values.

Table 5.2: GaAs measured NLA, and NLR

Sample	T(K)	Thickness (mm)	$\sigma_a$ ( $10^{-17} \text{ cm}^2$ )	$\gamma$ ( $10^{-13} \text{ cm}^2/\text{W}$ )		$\sigma_r$ ( $10^{-21} \text{ cm}^3$ )		$\beta$ (cm/GW)	
				This Work	Prior	This Work	Prior	This Work	Prior
GaAs	300	0.42	$5^{17}$	-20.0 $\pm 1\%$	$-4.1^{13}$ $-15^{14}$	-3.0 $\pm 13\%$	$-5.9^{13}$ $-0.4^{14}$	$25.5 \pm 11\%$ 17.6 (Theory)	$26^{13}$ $35^{14}$
GaAs	77	0.42	$5^{17}$	-13.0 $\pm 10\%$	-	-5.1 $\pm 9\%$	-	$23.1 \pm 14\%$ 15.7 (Theory)	-

The measured NLA and NLR coefficients for GaAs compare favorably with both theoretical values and previous experimental results. The magnitude of the nonlinear index of refraction measured in this research is higher than values measured previously, but comparable to at least one of the values. At 77 K, the  $\gamma$  value was found to be 35% smaller than the measured value at 300 K. The free

carrier refraction coefficient was also found to be different at the two temperatures, while the measured value at room temperature corresponded well with previous measurements. The two photon absorption coefficient is higher than the theoretical value but is consistent with prior results. As expected from the theoretical values, the two photon absorption coefficient decreased slightly when the temperature was brought down to 77 K.

#### **5.4 Measured NLA & NLR of InP**

A 1mm thick sample of InP was characterized using the irradiance scan technique at both 300 K and 77 K. Having characterized the nonlinear optical properties of GaAs, we observed a decrease in  $\beta$  with the decrease in temperature, as expected from theory. As before, spectra were taken of the sample at 300 K and 77 K, and it can be seen that the wavelength at which the sample begins transmitting decreases as the temperature decreases due to a band gap shift (Fig. 5.5). The transmission values at 1.064  $\mu\text{m}$  were very close, at 92% and 91% for 300 K and 77 K, respectively.

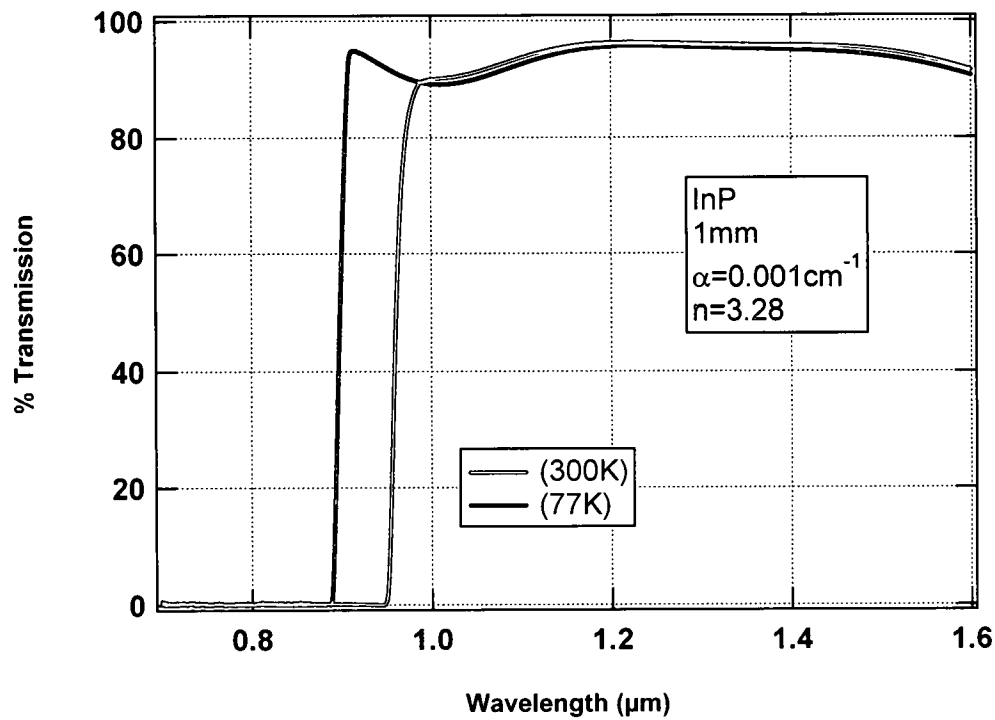


Fig. 5.5: InP spectra at 300 K and 77 K

The data sets used to determine the optical nonlinearities of the InP sample at 300 K and 77 K are shown in Figs. 5.6 and 5.7, respectively.

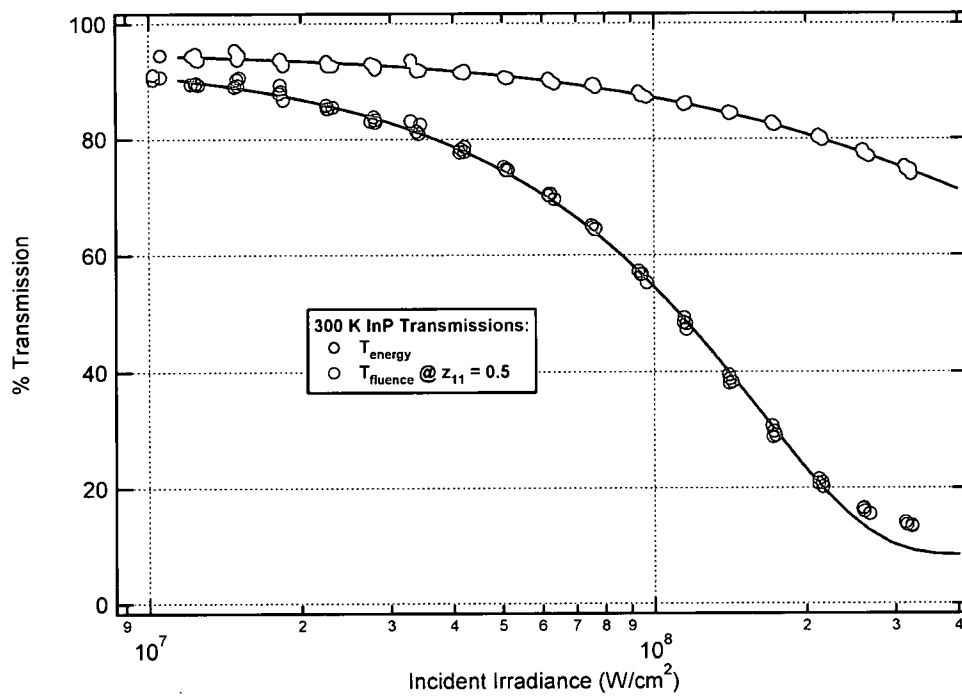


Fig. 5.6: InP NLA, and NLR at 300 K

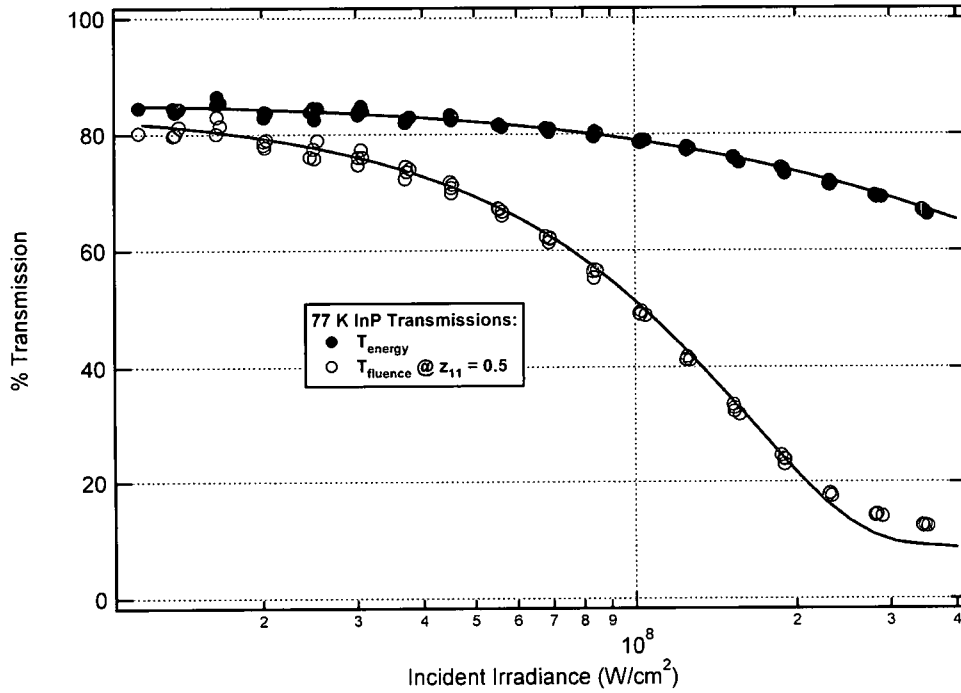


Fig. 5.7: InP NLA, and NLR at 77 K

The NLA and NLR values measured at both 300 K and 77 K are illustrated in Table 5.2. Little prior work has been published regarding the characterization of InP, including characterization at 300 K. Needless to say, like all semiconductors studied in this research, there are no available prior measurements at 77 K with which to compare.

Table 5.3: InP measured NLA, and NLR

				$\gamma$ ( $10^{-12}$ cm <sup>2</sup> /W)		$\sigma_r$ ( $10^{-21}$ cm <sup>3</sup> )		$\beta$ (cm/GW)	
Sample	T(K)	Thickness (mm)	$\sigma_a$	This Work	Prior	This Work	Prior	This Work	Prior
InP	300	1.0	-	-1.2 $\pm 47\%$	-1.5 <sup>14</sup> $\pm 30\%$	-4.3 $\pm 10\%$	-0.4 <sup>14</sup>	28.5 $\pm 3\%$ 23.4 (Theory)	90 <sup>14</sup> $\pm 50\%$
InP	77	1.0	-	-1.0 $\pm 50\%$	-	-5.7 $\pm 7\%$	-	28.2 $\pm 2\%$ 21.1 (Theory)	-

The magnitude of the nonlinear index of refraction decreases insignificantly when the temperature is changed from 300 K to 77 K and the magnitude of the free

carrier refraction coefficient increases with this change. The measured two photon absorption coefficient for both temperatures was found to be higher by ~20% than the full band structure theoretical calculation. The only experimentally determined InP  $\beta$  value we were able to find in the literature was significantly higher than theory and had a very large relative uncertainties. Consequently, comparison of our results to these measurements is of little value.

### 5.5 Measured NLA & NLR of CdTe

The spectra shown in Fig. 5.8 were taken of a 6.21 mm thick sample of CdTe. As with GaAs and InP, the transmission cut-on was observed to shift to a shorter wavelength at low temperatures.

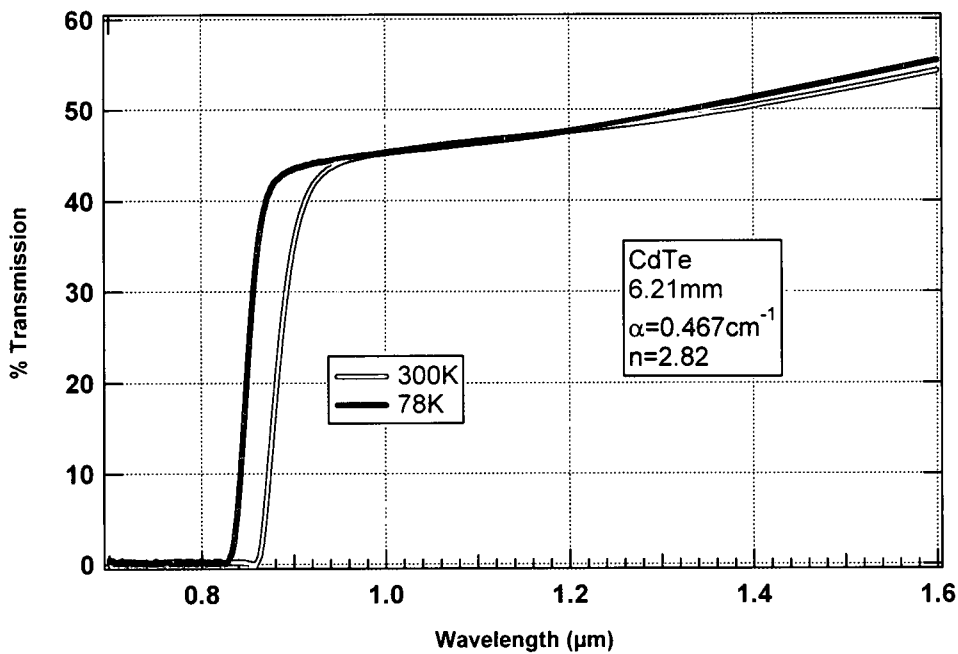


Fig. 5.8: CdTe spectra at 300 K and 77 K

Figs. 5.9 and 5.10 show the data collected and the associated fits that were used to determine the optical nonlinearities of CdTe at 300 K and 77 K.

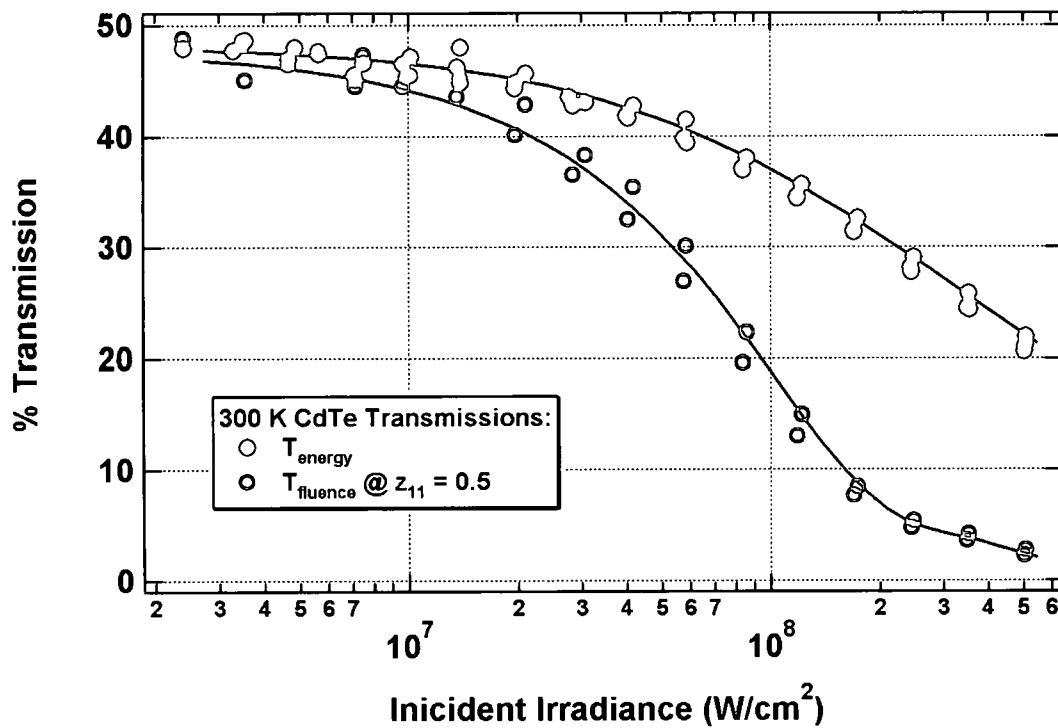


Fig. 5.9: CdTe NLA, and NLR at 300 K

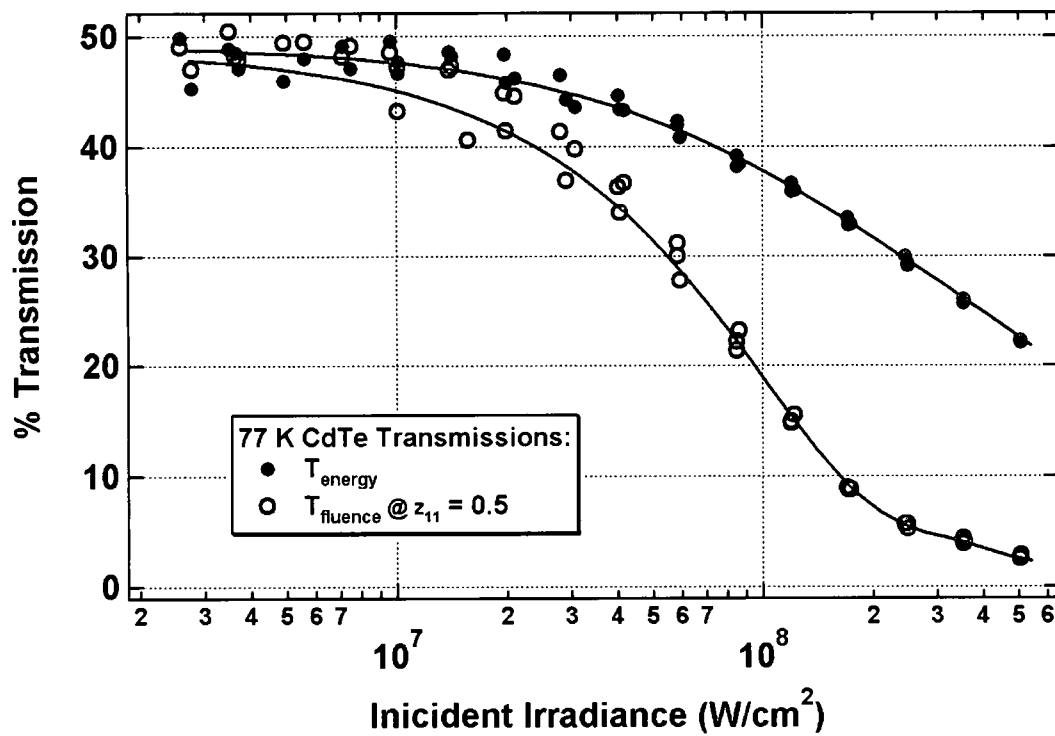


Fig. 5.10: CdTe NLA, and NLR at 77 K

The NLA and NLR values measured in this research for CdTe are tabulated in Table 5.4

**Table 5.4: CdTe measured NLA, and NLR**

				$\gamma$ ( $10^{-14}$ cm <sup>2</sup> /W)		$\sigma_r$ ( $10^{-21}$ cm <sup>3</sup> )		$\beta$ (cm/GW)	
Sample	T(K)	Thickness (mm)	$\sigma_a$	This Work	Prior	This Work	Prior	This Work	Prior
CdTe	300	6.21	-	-15 $\pm 25\%$	-27 <sup>13</sup>	-4.2 $\pm 20\%$	-5.2 <sup>13</sup>	23.4 $\pm 3\%$ 25.1 (Theory)	26.1 <sup>13</sup>
CdTe	77	6.21	-	-9.0 $\pm 25\%$	-	-4.1 $\pm 20\%$	-	19.6 $\pm 4\%$ 21.1 (Theory)	-

The nonlinear index of refraction measured at 300 K for CdTe agrees with prior measurements. We found that the magnitude of  $\gamma$  decreased when the temperature was lowered to 77 K. The free carrier refraction coefficient found for CdTe in this research corresponds well with previous measurements at room temperature. No significant change was observed in  $\sigma_r$  when the material was decreased to a temperature of 77 K. The two photon absorption coefficient measured at 300 K agrees well with past results but is smaller than the two band theory indicates it should be. A decrease in the two photon absorption coefficient was observed for both GaAs and CdTe when the temperature was changed from 300 K to 77 K, an insignificant change was observed for InP.

## 5.6 Final Results Discussion

The nonlinear refractive index measurements for CS<sub>2</sub> agreed very well with previous results. As expected, no two photon absorption was detected using the irradiance scan technique for the CS<sub>2</sub> cell. The nonlinear optical properties of the CS<sub>2</sub> calibration sample compared favorably with past results,

indicating fits to  $\gamma$  were determined reliably in the absence of  $\beta$ . The reliability of the experimental technique was confirmed by the close correspondence the values reported here at 300 K and those measured previously, for several different materials.

The nonlinear optical properties were measured for three semiconductors at both 300 K and 77 K using the irradiance scan method. For the most part, the nonlinear index of refraction and free carrier refraction coefficient measured for GaAs and CdTe agreed with values found in the past using alternate measurement techniques. For InP, the nonlinear refractive index and free carrier refraction coefficient were observed to diverge with respect to previously measured values.

The two photon absorption coefficient for both GaAs and CdTe agreed very well with past results. The two photon absorption coefficient for InP did not seem to change significantly at the two different temperatures, though a change was observed in GaAs and CdTe.

Several trends were observed in the nonlinear optical properties of the three semiconductors when the temperature was changed from 300 K to 77 K. The nonlinear index of refraction decreased in magnitude for two of the materials, decreasing by ~40% for both GaAs and CdTe, while a less significant change was observed for InP. For GaAs and InP the free carrier refraction coefficient increased in magnitude (by 30-70%), while in CdTe a significant change was not seen. Finally, while a decrease of ~10% in the two photon absorption coefficient



was observed for both GaAs and CdTe, an observed change in  $\beta$  for InP was not significant.

Some of the values presented in this chapter deviated from past measurements and theory. It is important to be confident that the obtained results are correct. The following chapter will discuss the overall performance of the Irradiance Scan and accuracy of its results.

## **Chapter 6**

### **System Performance & Accuracy**

#### **6.1 *Introduction***

In any experimental system, factors such as the linearity of the detection system, robustness of the computer algorithm used to process the data (taken in the presence of noise), and reproducibility of the experimental data all have an effect on the accuracy of the results. It is essential to develop an understanding of the accuracy of the test bed to understand the associated error in the measured nonlinear optical properties of materials characterized. The overall performance as well as the accuracy of measurements made using this system will be discussed in this chapter.

#### **6.2 *Linearity of Detection System***

An open aperture pyro-electric detector was used to measure the total transmitted energy. The total energy incident upon the sample was likewise monitored by an open aperture detector. The response of the total transmitted energy detector at varying incident energies is illustrated in Fig. 6.1.

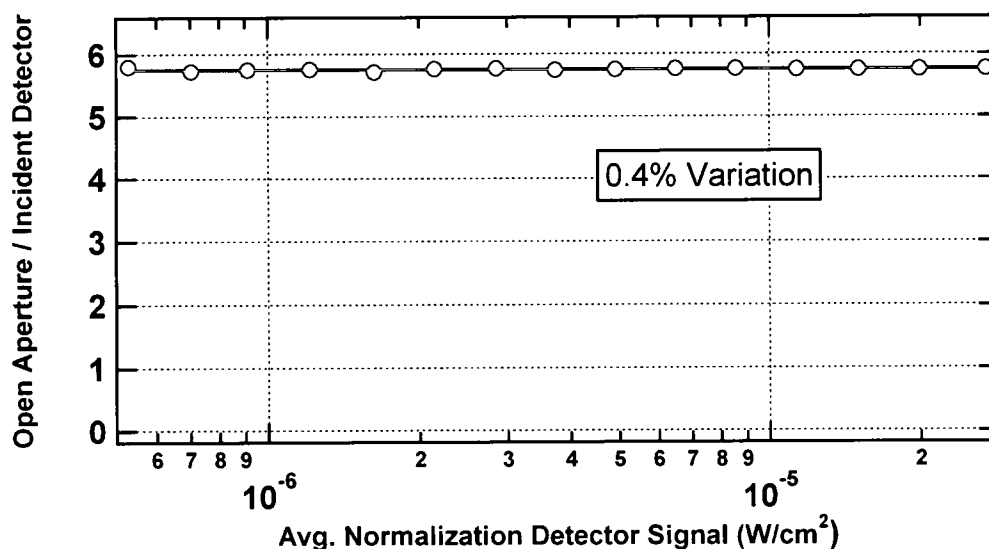


**Fig. 6.1: Total transmitted energy detectors response to varying incident energies**

This calibration shows that the pyro-electric used is indeed linear to within 0.4% over the dynamic range of the experiment. It can be seen from the plot that at low irradiance levels there is a small amount of noise present.

The detector response shown in Fig. 6.1 is valid when AR coated samples are characterized. When samples that are not AR coated are characterized, approximately half of the light is lost. As a result, the actual transmitted energy will cover a range involving smaller energies; this introduces more noise at low irradiance levels.

The total energy transmitted through the pinhole for the on-axis fluence detector was significantly smaller than that incident upon the total energy transmission detector. As a result, a silicon detector was chosen for its greater sensitivity. A silicon detector is good at measuring low intensity signals but it saturates easily. With proper attenuation using neutral density filters, a pinhole, and a filter to eliminate 120Hz noise from the overhead lights, the near flatline profile shown in Fig. 6.2 was achieved.

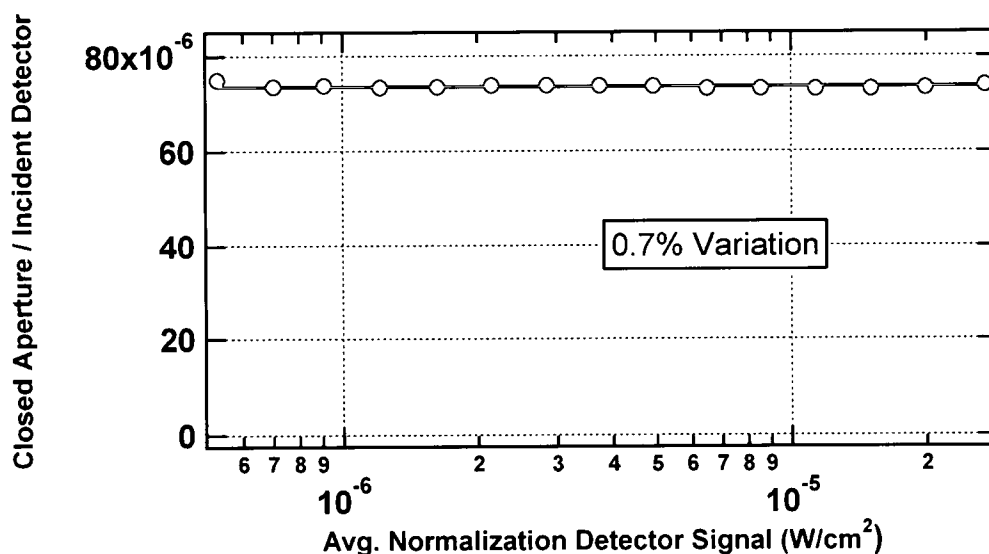


**Fig. 6.2: On-axis fluence detectors response to varying incident energies**

It can be seen that the on-axis fluence detector response to varying incident energies is nearly linear, having only a 0.7% variation. Noise, although minimal, is apparent at low irradiance levels on the on-axis fluence detector.

Overall, the detection system has a linear response across the range of energies incident upon the various detectors used to determine optical nonlinearities. It was of the utmost importance to have a detection system with a linear response; otherwise, nonlinearities of the detection system could be confused with optical nonlinearities in the materials under test.

### **6.3 Reproducibility**

It is essential to be able to measure consistent nonlinear optical properties between successive runs on a material. A temporal calibration drift has been observed, and this section will discuss what might be contributing to this and the reproducibility of results. Both closed and open aperture calibrations are taken before and after materials are characterized. Occasionally, we have observed different calibration factors before and after running a material sample. The turn

around time for running a sample is approximately 20 minutes. Comparing closed aperture calibration values taken approximately every 20 minutes over the course of a couple hours, we have observed fluctuations as high as 2.0%.

It has yet to be determined what is causing the fluctuation in the total transmitted energy detector. The calibration factor is the ratio of energy on the open aperture detector to the incident energy on the reference detector. Laser fluctuations should not be a problem and the detector is stationary in between calibrations, so positional dependencies should be eliminated. A fixed polarizer is used as part of the attenuation optics so polarization issues should not be present.

The position of the closed aperture detector is manually optimized by adjusting the detector position using a translation stage. The variation in position is likely attributable to the changing calibration values for the on-axis fluence detector. If any pointing jitter is present there is potential that the measured on-axis fluence could vary as the pointing of the laser changes (drift). Effectively, pointing jitter could cause the peak of the symmetric pulse profile to walk off the pinhole. It was thought that the half wave plate may be slightly wedged causing the beam to walk off the closed aperture detector as it was rotated; however, this was checked using a focal plane array (FPA) and found to not be an issue.

Issues have been observed regarding how cylindrically symmetric the profile actually is with a sample present in the system. This and other issues that contribute to the accuracy of the model will be discussed in detail in the following section.

## 6.4 Accuracy of Model

From the various transmission plots presented in Chapter 5, it can be seen that occasionally the fit generated for the on-axis fluence data does not fit the last few high fluence points very well. When high energy densities are incident on the material under test, the transmitted pulse profile is no longer cylindrically symmetric (Fig. 6.3).

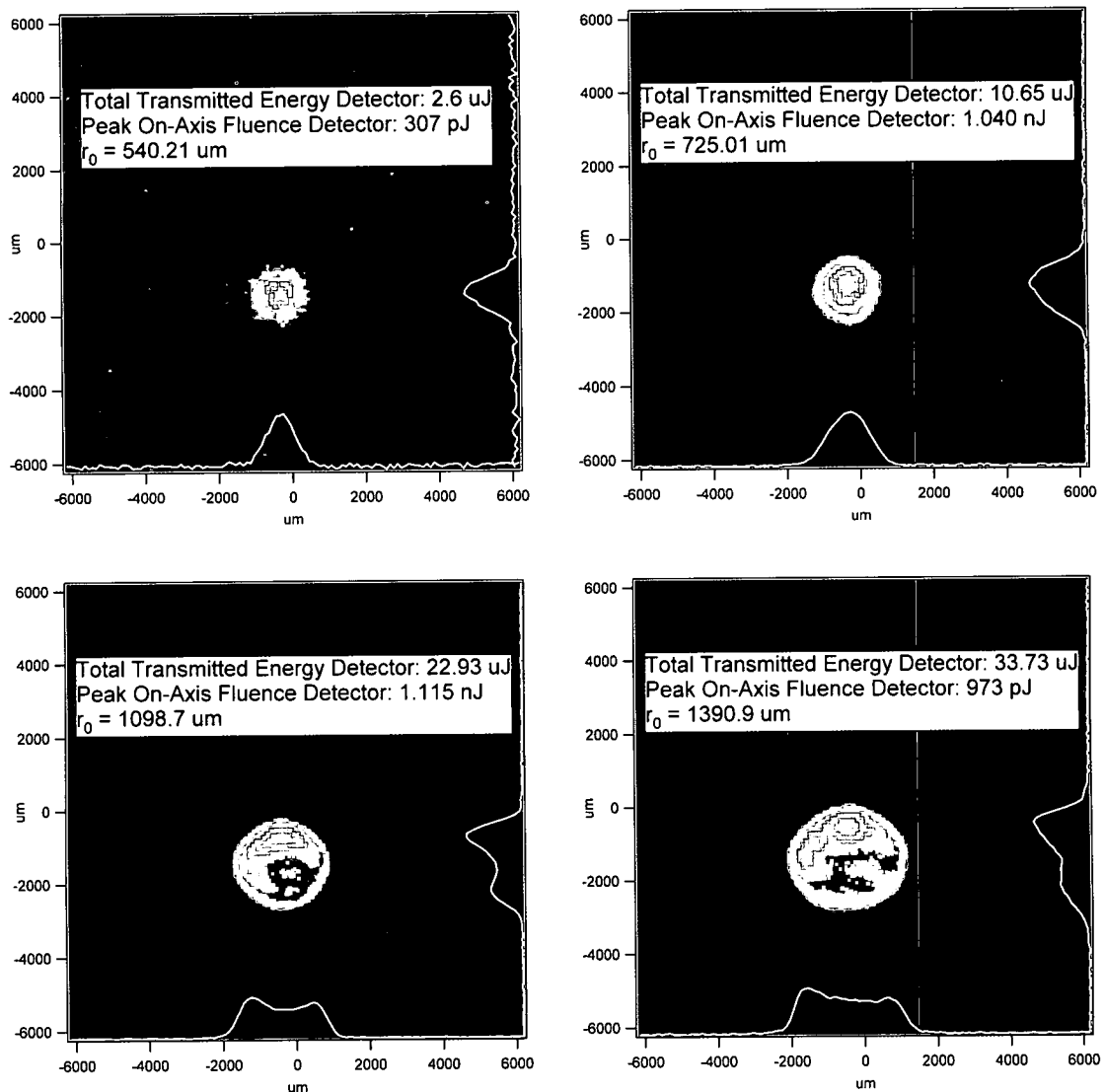


Fig. 6.3: On-axis fluence detectors response to varying incident energies

Fig. 6.3 depicts a sequence of images captured on a FPA showing the changing pulse profile for increasing incident irradiance levels on a 6.21 mm thick wafer of CdTe. These images also illustrate the negative lensing effect that occurs resulting from the nonlinear optical properties of the CdTe material. The position of the on-axis fluence detector is centered at low fluence levels and is kept fixed while the fluence is variably attenuated. The sequence of images illustrates how the correct on-axis fluence would not be measured at high fluence levels because the peak has shifted locations. The computer algorithm used to determine the NLR terms assumes a symmetric incident profile and a homogeneous medium. When the incident beam profile is no longer cylindrically symmetric, the model breaks down. Other than these last few points having high power densities, the fits for the on-axis fluence data fit the data very well.

The model also assumes a perfectly flat phase front at the front face of the sample. In practice, the phase profile is close to being flat. The question is how far phase profile can deviate before the model starts having problems. The pulse was spatially filtered so the phase profile should be relatively flat. The model assumes a perfectly Gaussian pulse profile at the first face of the sample, which may also contribute to the inconsistent fit. Like any laser, the profile of the beam is not perfectly Gaussian. A recent paper<sup>18</sup> shows that the input beam profile must be very close to Gaussian in order to measure optical nonlinearities accurately. Even small asymmetries in the beam profile have a large effect when high irradiances are incident on a nonlinear medium. The fits were a good match

for the data set except for the last few points, so we don't believe this is an issue in the results presented in this research.

Intra-sample diffraction is ignored in the model because the Rayleigh range is much greater than the sample thickness and we do not believe this is an issue in the fits. The sample under test may have inhomogeneities that could amplify filamentation of the beam; this may explain the characteristics of the images in Fig. 6.3. The samples tested in this research were rotated to see if there was any polarization effects noticed on the FPA. No polarization effects were observed or any type of change to the beam profile while the sample was rotated. It is likely variations in the amplitude and phase of the beam are causing discrepancies in the fit but inhomogeneities in the sample are not amplifying filamentation in the beam.

The following chapter will recapitulate the method of test and trends in the measured nonlinear optical properties of the sample set characterized. Also, work that has been planned to try to eliminate some of the discrepancies between the model and actual results will be discussed. Future goals of the project, where the research is headed, and how changes will be implemented will be covered in the chapter to follow.



## **Chapter 7**

### **Conclusions**

#### **7.1 Accomplishments**

The goal of this research was to construct a measurement system that could accurately measure the nonlinear optical properties of semiconductor materials at 300 K and 77 K. This was realized for three semiconductor materials: gallium arsenide, indium phosphide, and cadmium telluride.

The ability of the system to accurately measure a small nonlinear index of refraction was verified using CS<sub>2</sub>. The nonlinear index of refraction, free carrier refraction coefficient, and two photon absorption coefficients were measured at both 300 K and 77 K for each of the three semiconductors characterized. The measured values at 300 K correlated with measurements made in the past. The majority of measurements made at 300K and 77 K agreed with theoretical calculations. To the best of our knowledge, this was the first time nonlinear optical properties of GaAs, InP, and CdTe have been measured at 77 K. The results of this work are summarized in Table 7.1.

**Table 7.1: Summary of nonlinear optical properties measured in this research**

				$\gamma$ ( $10^{-13}$ cm <sup>2</sup> /W)		$\sigma_r$ ( $10^{-21}$ cm <sup>3</sup> )		$\beta$ (cm/GW)	
Sample	T(K)	Thickness (mm)	$\sigma_a$ ( $10^{-17}$ cm <sup>2</sup> )	This Work	Prior	This Work	Prior	This Work	Prior
CS <sub>2</sub>	300	25	-	3 ±4%	3.11 <sup>12</sup>	-	-	-	-
GaAs	300	0.42	5 <sup>17</sup>	-20.0 ±1%	-4.1 <sup>13</sup> -15 <sup>14</sup>	-3.0 ±13%	5.9 <sup>13</sup> 0.4 <sup>14</sup>	25.5 ±11% 17.6 (Theory)	26 <sup>13</sup> 35 <sup>14</sup>
GaAs	77	0.42	5 <sup>17</sup>	-13.0 ±10%	-	-5.1 ±9%	-	23.1 ±14% 15.7 (Theory)	-
InP	300	1	-	-1.2 ±47%	-1.5 <sup>14</sup> ±30%	-4.3 ±10%	-0.4 <sup>14</sup>	28.5 ±3% 23.4 (Theory)	90 <sup>14</sup> ±50%
InP	77	1	-	-1.0 ±50%	-	-5.7 ±7%	-	28.2 ±2% 21.1 (Theory)	-
CdTe	300	6.21	-	-15 ±25%	-27 <sup>13</sup>	-4.2 ±20%	-5.2 <sup>13</sup>	23.4 ±3% 25.1 (Theory)	26.1 <sup>13</sup>
CdTe	77	6.21	-	-9.0 ±25%	-	-4.1 ±20%	-	19.6 ±4% 21.1 (Theory)	-

For all three semiconductors, a decrease in magnitude of the nonlinear index of refraction was observed when the temperature of the sample was lowered to 77 K. The free carrier refraction coefficient increased in magnitude for GaAs and InP with the temperature change, while there was no significant change observed for the CdTe sample. The two photon absorption coefficients of GaAs and CdTe decreased when the temperature was lowered, and an insignificant change was observed for InP.

When compared with alternative methods, the irradiance scan had multiple advantages when measuring nonlinear optical properties of novel

materials. Since novel materials are often wedged, measurement techniques that require translation introduce issues such as beam walking. With the chosen method of characterization, beam walking was not a problem because the sample was fixed at the focus. An added advantage to keeping the sample fixed is that the bulky dewar and associated vacuum/electrical lines used for the cryogenic measurements could remain stationary. To the best of our knowledge, this was the first time the irradiance scan technique has been used to measure temperature dependent nonlinear optical properties of semiconductors.

The method of test developed in this research allows an experimenter to characterize a novel material's temperature dependent nonlinear optical properties accurately. It is expected that the system will prove extremely valuable for material characterization.

## **7.2 Future Goals**

Having demonstrated the ability of the irradiance scan method to accurately measure temperature dependent nonlinear optical properties of semiconductors, there are several future goals for this research. The immediate goal of the project is to measure the nonlinear optical properties of additional materials at 300 K and 77 K at the  $1.064\mu\text{m}$  wavelength. Another short term goal is to better characterize the irradiance scan method and determine the optimal  $z_{11}$  position experimentally, as well as performing a full optimization characterization theoretically. Once this is complete, the nonlinear optical properties of materials in the midwave infrared will be characterized at temperatures ranging from 77 K to 300 K.

To create picosecond pulses in this wavelength range a difference frequency generator (DFG) and optical parametric amplifier (OPA) will be required. The 1.064 $\mu$ m laser utilized in this research will be mixed using nonlinear processes creating different wavelength pulses that are then amplified by the OPA.

It is desirable to be able to switch between different wavelength pulses quickly, so the setup shown in Fig. 7.1 was constructed; this should allow characterization to be done from 680nm-10 $\mu$ m relatively quickly.

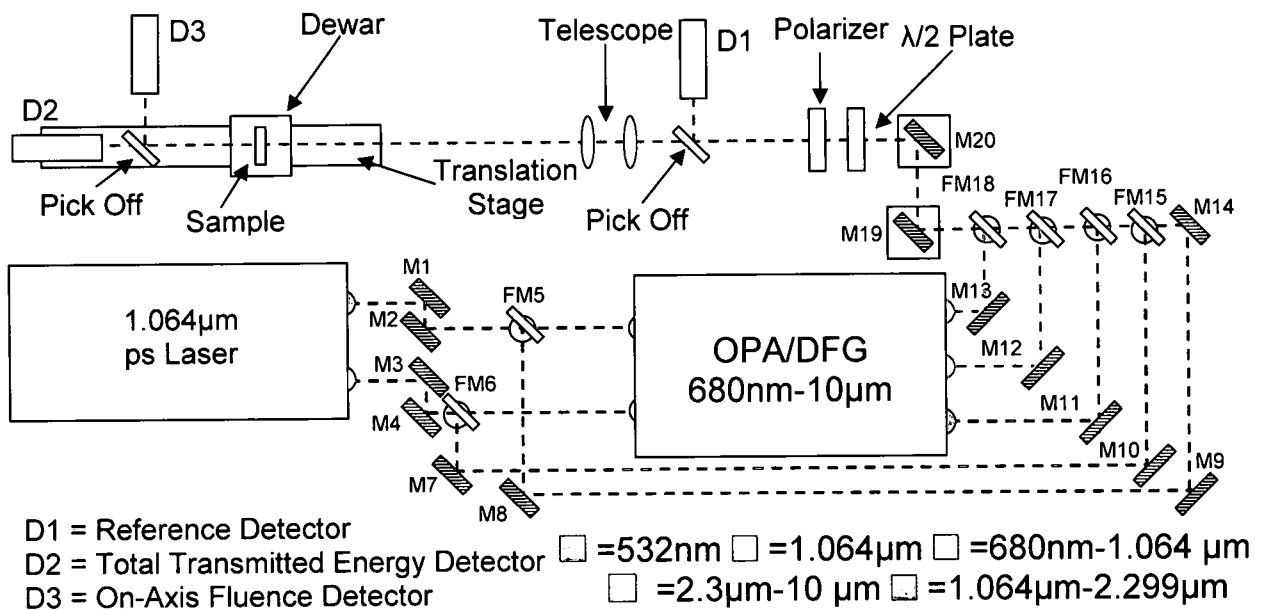


**Fig 7.1: 680nm-10 $\mu$ m irradiance scan test bed**

A series of flipper mirrors (FM) are used to route different wavelengths of light into the test system. The configuration of flipper mirrors for a desired wavelength pulse are shown in Table 7.2.

**Table 7.2: Mirror configurations**

	M5	M6	M15	M16	M17	M18
532nm Pump	Up	Down	Down	Down	Down	Down
1.064 $\mu$ m Pump	Down	Up	Up	Down	Down	Down
680nm-1.064 $\mu$ m	Down	Down	Down	Down	Down	Up
2.3 $\mu$ m-10 $\mu$ m	Down	Down	Down	Down	Up	Down
1.064 $\mu$ m-2.299 $\mu$ m	Down	Down	Down	Up	Down	Down

Because the focus of the telescope will change as a function of wavelength, the dewar was mounted on a translation stage to allow the front face of the material under test to be brought to focus quickly. An FPA will be used to measure the on-axis fluence. Using a large area FPA and an algorithm to find the centroid will eliminate error introduced by manually optimizing the detector position. This versatile system will allow us to measure temperature and wavelength dependent nonlinear optical properties over a large spectrum.

## References

- [1] E. VanStryland, H. Vanherzeele, M. Woodall, M. Soileau, A. Smirl, S. Guha, and T. Boggess, "Two photon absorption, nonlinear refraction, and optical limiting", *Opt. Eng.* **24**(4), 613-623 (1985).
- [2] M.J. Weber, *Handbook of Laser Science and Technology Volume III Optical Materials: Part 1*, (Florida: CRC Press, 1986), p. 229-258.
- [3] M. Sheik-Bahae, "Measurement of nonlinear index by a relay-imaged top hat Z-scan technique", *SPIE* **27**(14), 52-60 (1989).
- [4] P. Chen, "A two dimensional Z-scan method for the measurement of optical nonlinear effects", *SPIE* **31**(46), 160-168 (1998).
- [5] Micheal. Moran, Chiao. She, and Robert. Carman, "Interferometric measurements of nonlinear refractive-index coefficient Relative to CS<sub>2</sub> in laser-system-related materials", *IEEE Jour. of Quan. Elect.* **11**(6), 259-263 (1975).
- [6] B. Taheri, H. Liu, R. Powell, and J. Song, "Intensity scan and two photon absorption and nonlinear refraction of C<sub>60</sub> in toluene", *Appl. Phys. Lett.* **68**(10), 1317-1319 (1996).
- [7] W. Lee Smith, "Two photon absorption in condensed media," *Handbook of Laser Science and Technology*, p. 229-234, 1986.
- [8] P. Klocek, M.W. Boucher, J.M. Trombetta, and P.A. Trotta, "High resistivity and conductive gallium arsenide for IR optical components", *Window and dome technologies III*, SPIE p74-85 (1992).
- [9] E. Bente, and M. Smit, "Ultrafast InP optical integrated circuits", *SPIE Vol.* 6124 (2006).
- [10] R. Mostefaouia, S. Belarbia, and A. Benatallah, "Optical study of a solar cell" *Science Direct*, 209, 10-14 (2007).
- [11] S. R. Friberg and P. W. Smith, Nonlinear optical glasses for ultrafast optical switches, *IEEE J. Quant. Electron* QE23:2089 (1987).

R002593671

- [12] S. R. Friberg and P. W. Smith, Nonlinear optical glasses for ultrafast optical switches, *IEEE J. Quant. Electron* QE23:2089 (1987).
- [13] A. A. Said, M. Sheik-Bahae, T. H. Wei, J. Young, and E. Van Stryland, "Determination of bound-electronic and free-carrier nonlinearities in ZnSe, GaAs, CdTe, and ZnTe," *J. Opt. Soc. Amer. B* **9**(3), pp. 405–14, 1992.
- [14] M.D. Dvorak and B.L. Justus, "Z-scan studies of nonlinear absorption and refraction in bulk, undoped InP", *Optics Communications*, **114**, 147, 1995.
- [15] S. Krishnamurthy, L. Gonzalez, S. Guha, "Accurate evaluation of nonlinear absorption in InAs, InSb, and HgCdTe alloys," *J. of Apl. Phys.* **101**(113104), 2007.
- [16] Z. Liu, Y. Liu, B. Zhang, W. Zhou, J. Tian, W. Zang, and C. Zhang, "Nonlinear absorption and optical limiting properties of carbon disulfide in a short-wavelength region," *J. Opt. Soc. Am. B* **24**, 1101-1104 (2007).
- [17] MSM Database, (2005), [www.ioffe.rssi.ru](http://www.ioffe.rssi.ru) Semiconductor Properties, Retrieved February 29, 2008 from [www.ioffe.rssi.ru/SVA/NSM/Semicond/GaAs/optic.html](http://www.ioffe.rssi.ru/SVA/NSM/Semicond/GaAs/optic.html).
- [18] V. Dubikovskiy, D. J. Hagan, and E. W. Van Stryland, "Large nonlinear refraction in InSb at 10 $\mu$ m and the effects of Auger recombination", *J. Opt. Soc. Amer. B* **25**(2), pp. 223-235.